Mater.Phys.Mech.3 (2001) 63-100

# ROLE OF MESOSTRUCTURE EFFECTS IN DYNAMIC PLASTICITY AND STRENGTH OF DUCTILE STEELS

**Yu.I. Mescheryakov, A.K. Divakov and N.I. Zhigacheva**

Institute of the Mechanical Engineering Problems, Russian Academy of Science,
V.O. Bolshoj 61, Saint-Petersburg, 199178, Russia

*Received: December 11, 2000*

**Abstract.** Dynamic deformation and fracture of solids are known to be the multiscale processes. Mesolevel-1 relates to deformation modes inside the structure elements while mesolevel-2 is self-consistent motions of conglomerates of the elements. Shock experiments and molecular dynamics simulation show a presence of local strain rate fluctuations (dispersion) which sensitively depend on the non-equilibrium of deformation process. Velocity dispersion at the mesolevel-1 ($D^2_{m1}$) characterizes a relaxation of local stresses while the dispersion at the mesolevel-2 ($D^2_{m2}$) is responsible for fragmentation of material. When $D^2_{m1} = D^2_{m2}$ fragmentation is suppressed and material reveals maximum strength. At the unsteady stages of straining the particle velocity acquires defect of velocity which characterizes an intensity of energy exchange between scale levels. In the present paper the energy exchange is considered from the position of spallation. For five kinds of steel it is shown that spall-strength is maximum when the velocity dispersion at the mesolevel equals defect of the average velocity. Criterion for spallation takes into account the energy exchange between scale levels.

## 1. INTRODUCTION

One of primary problems in the dynamics of materials is a coupling between microstructure features of a material and its macroscopic response on impact. A lot of theoretical models based on the microstructure dynamics, in particular on dislocation dynamics, has been developed to describe the macroscopic behavior of material both under uniaxial stress and uniaxial strain conditions. Nevertheless, this coupling is poorly understood both qualitatively and quantitatively. This is due to commonly used wrong approach when one tries to link the resulting macroscopic response on impact with the data on the microstructure state obtained *after* dynamic loading.In reality, adequate mathematical modeling of dynamic processes should be based on the microstructure kinetics data obtained in real time, i.e. *during* the dynamic deformation and fracture processes. This requires that experimental technique at hand must provide a measuring not only macroscopic response of specimen on impact such as the time-resolved free surface velocity profile but also kinetic characteristics of internal structure. These characteristics provide an information on the relative mobility of elementary carriers of deformation (ECD). Since the motion of ECD in heterogeneous medium has a specifically stochastic nature, their kinetics in common case must be described on the language of the particle velocity distribution function or its statistical moments. The first statistical moment is known to be a mean particle velocity. It characterizes an averaged (flux) motion of medium with some mean velocity *u.* Random character of the particle velocity reflects the second statistical moment – particle velocity dispersion $D^2$.

It is generally now recognized that direct transition from dislocation dynamics to macroscopic plasticity is not possible because of collective interactions in dislocation ensembles and incorporating into plastic flow large-scale carriers of deformation. In the shock wave propagation phenomena that conclusion has been made after numerous unsuccessful attempts to describe the elastic precursor decay through dislocation dynamics [1]. Collective interaction of dislocations results in for-

Corresponding author: Yu.I. Mescheryakov, e-mail: yum@fracture.ipme.ru

mation some intermediate scale of deformation, the so-called mesoscopic level [2,3]. All the events responsible for the change of kinematical mechanism of deformation depending on external loading and boundary conditions are thought to be realized at the mesolevel.

In considering the microstructure aspects of dynamic deformation and fracture it should be also confessed that experimentally determinable kinetic characteristics to date are those belonging to the mesoscopic scale level. However, as distinct from the static and quasistatic situation, in dynamically loaded medium mesolevel is not formed structure. It is specifically transient structure where a scale of ECD and energy capacity of mesoscopic scale level currently change depending on the degree of nonsteadiness of deformation process. Energy capacity of mesolevel characterizes a part of kinetic energy, initially given to body from external load, which is transferred to mesolevel in the form of velocity scattering of elementary carriers of deformation (mesoparticle velocity dispersion). In the unsteady plastic waves there exists a current energy exchange between meso- and macrolevel. At the load front of compressive pulse the average (flux) motion of medium is transformed into a velocity distributed motion of mesoparticles. This occurs in the form of decrease of average particle velocity resulting in the so-called fluctuative decay of shock wave [4]. On the contrary, during the release stage of dynamic loading decrease of dispersion leads to increase of mean particle velocity.

The objective of present paper is to find relationship between macroscopic response of materials to impact and microstructure kinetics. As a materials with different dynamic properties we use five kinds of ductile steel having different chemical composition and different thermal treatment: (1) – 40XHCMA steel, (2) – 38XH3MΦA steel, (3) – 4043 steel, (4) – 28XCH3MBΦA steel and (5) – 16X11H2B2MΦ steel (Russ. steel classification).

As a macroscopic strength-characteristic we use the spall-strength which is known to characterize an incipient strength of material under shock tension. That characteristic can be inferred from the free surface velocity profiles obtained in the plane collision tests [5]. To date a study of spallation seems to be the only possibility for investigation of peculiarities of material fracture at the micro and sub-microsecond range of tension loading.

The quantitative characteristic of microstructure kinetics here is a particle diffusion velocity (or the square root of the particle velocity dispersion) at the mesoscopic scale level. This characteristic is determined in real time in every and each shock loading. The so-called “decay”, or decrease of the free surface velocity at the plateau of compressive pulse serves as an additional experimental characteristic of the response of material to impact.

Section 2 is devoted to theoretical approach based on the statistical description of dynamically deformed medium. Section 3 includes the experimental technique and experimental results of dynamic tests of steels. Section 4 is results of microstructure investigations of post shocked specimens of steels and Section 5 is devoted to analysis of obtained results in the light of our theoretical approach.

## 2. STOCHASTIC APPROACHES TO MESOSTRUCTURE DESCRIPTION

### 2.1. Velocity Distribution Function and Its Statistical Moments.

Dynamic straining and fracture, including spallation, consists of acceleration stage, steady phase and stage of deceleration. Experiments on shock loading of solids using interference technique for measuring free surface velocity and particle velocity distribution histories in real time show:

- There is a non-equilibrium particle velocity distribution at the first and third stages of dynamic straining at the mesoscopic scale level while at the steady stage the velocity distribution is equilibrium. This means that behavior of solid at the steady stage corresponds to continuum medium while unsteady stages of dynamic processes must be analyzed in the frame of kinetic approaches.
- At the acceleration stage, together with increase of the particle velocity dispersion, a decrease of the average particle velocity takes place.
- At the deceleration stage simultaneously with decrease of velocity dispersion there is an increase of the average (macroscopic) particle velocity.

Mentioned above dependence of macroscopic particle velocity on the particle velocity distribution is the fundamental feature of unsteady processes in the structured media. The specifics of structure re-arrangement of dynamically deformed material reveals via the decrease (decay) of the average (macroscopic) particle velocity. The value of the velocity decay characterizes an intensity of energy exchange between macro- and meso-levels. Physically the particle velocity decay means that certain part of kinetic energy of macroscopic motion of medium is transferred to individual particles at the mesolevel. As a result, the particle velocity disper-

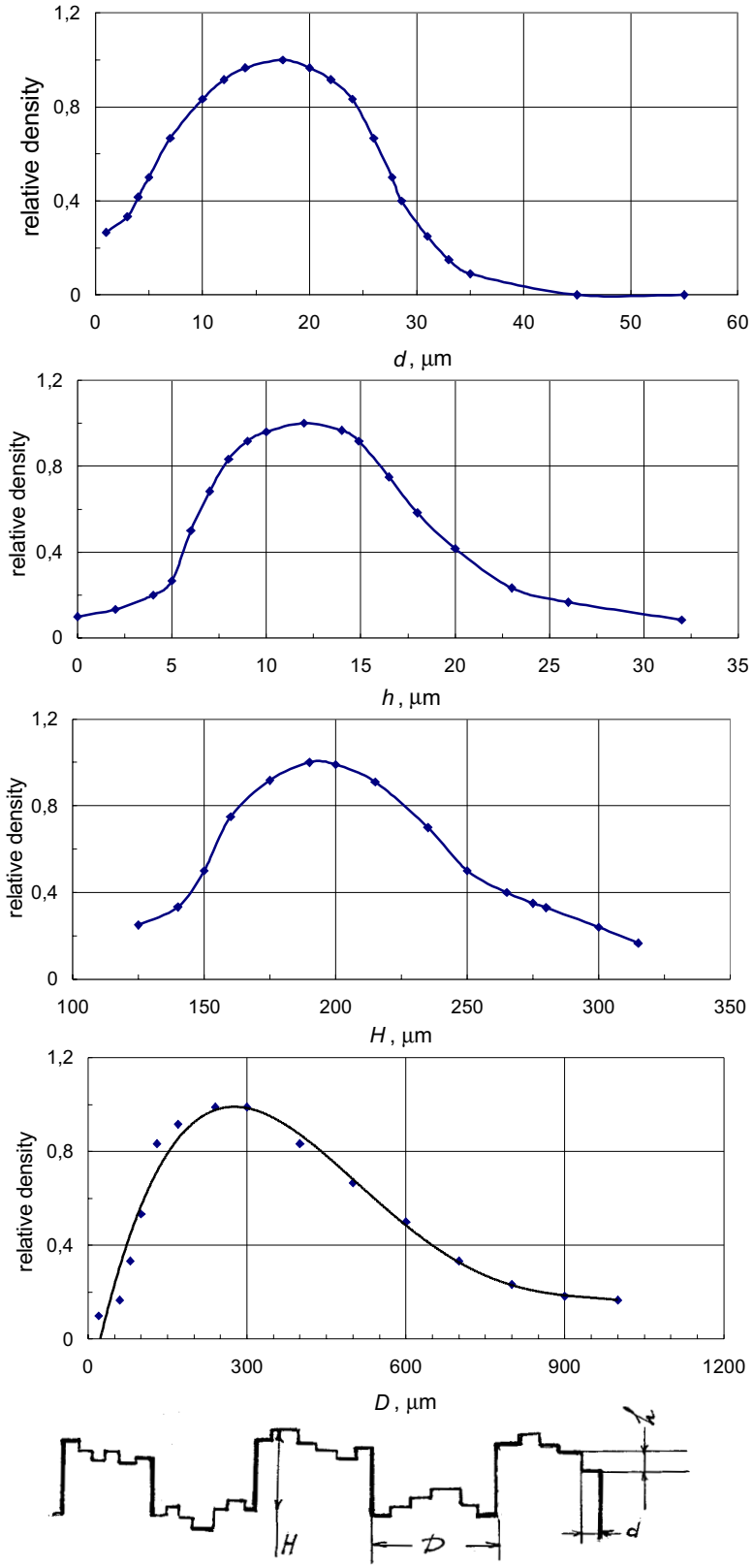


**Fig.1.1.** Experimental two-scale distributions for longitudinal and transverse steps of spallation for 30XH4M steel, [6].

sion at the mesolevel increases while the average velocity decreases.

Sometimes the mesoscopic scale level of deformation and fracture is subdivided by two sublevels. So, microstructure investigations of spall zone for

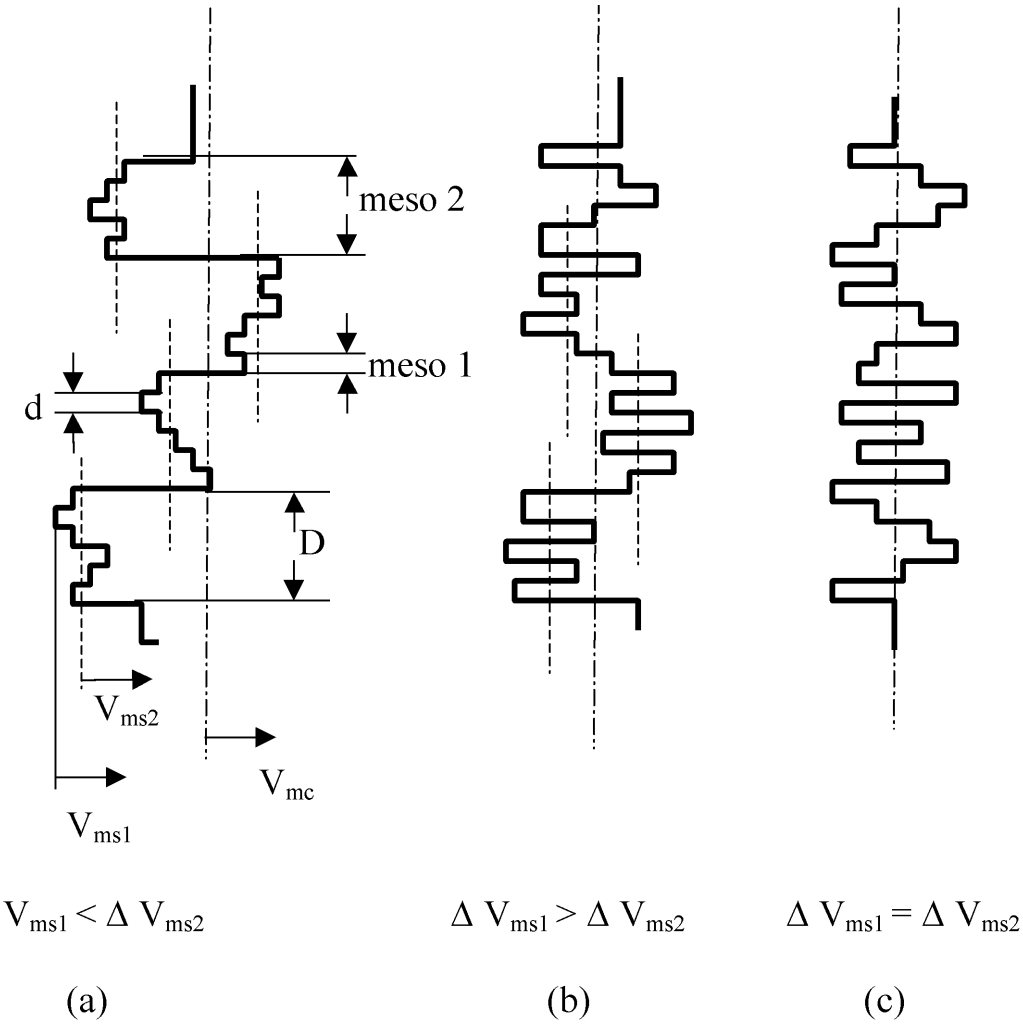


**Fig.1.2.** Space-velocity positions of wave front in heterogeneous medium.

30XH4M steel [6] shows that two scale levels take part in the dynamic fracture of this steel: mesolevel-1 (10-20 μm ) and mesolevel-2 (100-500 μm). In Fig. 1.1 the experimental distributions of elementary steps of spall cracking are presented for horizontal *(d* and *D)* and vertical (*h* and *H)* pieces of spall gap. This statistics shows that spallation of this material performs upon two scale levels simultaneously.

Elementary carriers of deformation and fracture for these sublevels may suffer their own particle velocity distributions. In this case there may be three different situations depending on the degree of the velocity distribution at these levels:

– Particle velocity dispersion at the mesolevel-1 is greater that at the mesolevel-2.
– Particle velocity dispersion at the mesolevel-2 is greater than at the mesolevel-1.
– Dispersions at these levels equal each other.

Above cases are presented in Fig.1.2 in the form of velocity-space phase configurations. The laser beam of interferometer which being focused on the free surface of target just corresponds to the meso-2 scale level. In other word, by using the laser interference technique, one obtains the velocity history for the individual element of mesolevel-2 only. This means that the macroscopic particle velocity *u,* which results from averaging the particle velocity distribution at the mesolevel-2, coincides with the average particle velocity at the mesolevel-1 only when the particle velocity dispersion for the meso-1 and meso-2 scale levels equal each other. For all the other cases the macroscopic velocity can be obtained only from averaging velocity distribution at the mesolevel-2. For that purposes L. M. Barker used a monitoring of the free surface of target in seven points simultaneously [7].

Microstructure investigation of post-shocked specimens show: even if at the macrolevel a process of dynamic straining flows under one-dimensional conditions, motion of elementary carriers of deformation at the mesolevel is particularly three-dimensional. Moreover, due to continuity conditions at the mesolevel the presence of the particle velocity distribution automatically means the fact of three-dimensional character of straining. As a result, such a kind of kinematical mechanisms of deformation and fracture as dynamic rotation can be realized at the mesolevel.

Description of non-equilibrium processes is known to be grounded on the concept of physical kinetics for the so-called particle velocity distribution function (or probability density) commonly used in the mechanics of fluid and gas. According to definition of the particle velocity distribution function value $f(\boldsymbol{r},\boldsymbol{v},t)\,d\boldsymbol{v}\,d\boldsymbol{r}\,dt$ means the mathematical expectation of the number of particles in the volume $d\boldsymbol{r}$ at the moment from $t$ to $t+dt$ with the velocities in the range from $\boldsymbol{v}$ to $\boldsymbol{v}+d\boldsymbol{v}$. Normalization condition requires that integrating over the velocity space would give the total number of particles

$$\int_{-\infty}^{\infty} f(\boldsymbol{r},\boldsymbol{v},t)\,d\boldsymbol{r}d\boldsymbol{v} = N. \tag{2.1}$$

The latter assertion is valid only for one kind of elementary carriers of deformation at the mesolevel. In reality mesostructure includes several kinds of carriers of deformation and every kind must be characterized by a individual distribution function $f_a(\boldsymbol{r}, \boldsymbol{v}_a, t)$. Then the normalization condition for such a kind of distribution looks as

$$\int f_a(\boldsymbol{r},\boldsymbol{v},t)\,d\boldsymbol{r}d\boldsymbol{v} = N_a, \tag{2.2}$$

where $N_a$ is the number of mesoparticles of kind $a$ (here and further integrating limits are omitted). From the normalization condition it follows that the value $n_a(r, t)$ which is determined by the relation

$$\int d\boldsymbol{v}\, f_a(\boldsymbol{r},\boldsymbol{v},t) = n_a(\boldsymbol{r},t), \tag{2.3}$$

means the density of particles number for kind $a$. For the mass density one obtains:

$$\rho(\boldsymbol{r},t) = \sum m_a n_a = \sum m_a \int d\boldsymbol{v}\, f_a(\boldsymbol{r},\boldsymbol{v},t). \tag{2.4}$$

Hydrodynamic flow of medium is characterized by the velocity of mass transportation. Define the mean mass velocity by relation:

$$u(r,t) = \frac{1}{\rho}\sum_a m_a n_a(r,t)\langle v_a\rangle, \tag{2.5}$$

where

$$\langle v_a\rangle = \frac{1}{n_a}\int \boldsymbol{v}_a f_a(\boldsymbol{r},\boldsymbol{v},t)\,d\boldsymbol{v}_a. \tag{2.6}$$

Besides the flow transportation of material there exists a relative motion of particles with the velocity

$$C_a = \Delta v_a(\boldsymbol{r},\boldsymbol{v},t) = \boldsymbol{v}_a - \boldsymbol{u}(\boldsymbol{r},t). \tag{2.7}$$

Its average value

$$\frac{1}{n_a(\boldsymbol{r},t)}\int f_a(\boldsymbol{r},\boldsymbol{v},t)(\boldsymbol{v}_a - \boldsymbol{u})d\boldsymbol{v} = \langle \Delta v_a(\boldsymbol{r},t)\rangle = \langle \boldsymbol{v}_a - \boldsymbol{u}(\boldsymbol{r},t)\rangle \tag{2.8}$$

calls a *diffusion velocity*.

Lastly, introduce once more characteristic of mesoparticle displacements of separate components of mesostructure which defines the impulse transportation.

Flow density of $x$ – projection of impulse for $a$ – component of mesostructure (relatively hydrodynamic flow) equals:

$$m_a \int d\boldsymbol{v}_a f_a c_{ax} c_a \equiv m_a n_a < c_{ax} c_a >.$$

Transportation of all the impulse projections is characterized by the tensor

$$P_{a,ik} = m_a n_a < c_{ax} c_a >, \tag{2.9}$$

which defines the kinetic stress tensor. In the gas dynamic it is accepted that tensor $\boldsymbol{P}(\boldsymbol{r}, t)$ is symmetrical. In dynamically deformed solid that assertion is really correct only for the macroscopic scale level. As for the mesolevel, the diffusion velocity components are not identical in different directions both due to non-isotropy of material and non-uniform space scattering of non-local correlations for the elementary carriers of deformation. As a result, non-equilibrium particle velocity distribution function becomes non-symmetrical, which results in asymmetry of the stress tensor. In turn, that asymmetry can initiate dynamically induced couple stresses at the mesolevel.

One of the first steps in developing the kinetic theory of either medium including mesostructure is

known to be a definition of the equilibrium distribution function. In the gas and fluid kinetics for that purpose the so-called local maxwellian distribution function is commonly used:

$$f^0_{LM}(\boldsymbol{r},\boldsymbol{v},t) = n\left(\frac{m}{2\pi kT}\right)^{3/2} \exp\left[-\frac{m(v-u)^2}{2kT}\right], \quad (2.10)$$

where $n$ is a function of coordinates and temperature. In the case of mesostructure one can use an analogy with kinetic theory of gases replacing coefficient ($m/2kT$) by the mesoparticle velocity dispersion $D^2$ [8]**:**

$$f^0(\boldsymbol{r},\boldsymbol{v},t) = n(\boldsymbol{r},t)\frac{\pi^{-3/2}}{D_1D_2D_3} \times \exp\left[-\sum\frac{(v_i - u_i(r,t))^2}{D_i^2}\right], \quad (2.11)$$

where $n(\boldsymbol{r},t)$ is a mean density of mesoparticles, $u_i(\boldsymbol{r},t)$ is the $i$-component of the mass velocity, and $D_i(\boldsymbol{r},t)$ is a mean dispersion of $i$-component of the mass velocity. In other words, particle velocity dispersion play a role of “temperature” of mesolevel. Sometimes in the West literature, in particular in the molecular dynamics simulation, it calls a “granular temperature”.

The first statistical moment of the PVDF, i.e. average particle velocity $u(r,t)$ characterizes the macroscopic behavior of medium under dynamic strain conditions.

Commonly used free surface velocity profiles measured by means of gauges or “VISAR” contain information about average behavior of material only. As for the mesoscopic effects such as shear banding and/or mesorotations, they are determined by the statistical moments of more higher order, such as particle velocity dispersion and excess, asymmetry of the velocity distribution function. Their values characterize the relative velocities of mesoparticles, though in the statistical meaning. This means that when speaking about mesoparticle dispersion under conditions of dynamic deformation, one cannot determine concretely a kind of elementary carriers of deformation at the mesolevel - dislocation groups, shear bands, tilt boundaries, rotations and so on. Furthermore, the concept of mesoparticle in the dynamically deformed body is thought to have a field sense. Dynamic mesoparticles can be considered as field fluctuations of mass velocity or local strain rate.

At the same time it is not too hard to estimate their typical scale by using the principles of interference measuring the particle velocity dispersion. Measurement of the particle velocity dispersion is based on the concept that different particles at the free surface of target within laser beam spot give different Doppler frequency shifts. Effective interaction of separate particle and laser radiation is really possible only in case if dimension of particle is more greater than laser radiation wave-length (approximately ten times). On the other hand, uniform widening of radiation spectrum is achieved only if within laser beam spot $d_b$ on the free surface of target there is a sufficient number of similar particles. From here the following estimate for dimension of particle $d_p$ can be inferred:

$$\lambda << d_p << d_b. \quad (2.12)$$

As a rule, being focused on the free surface of target, the laser beam has a transverse dimension about 70-100 μm while the laser radiation wavelength equals approximately 0.5-1.0 μm. Then the size of particle lies within interval of 7-10 μm. In accordance with a classification considered in [2] this size belongs to mesoscopical scale level.

Mesoparticle velocity distribution resulting in widening the laser radiation spectrum leads in turn to decrease of the interference fringe contrast, which gives a quantitative information on the particle velocity dispersion [9,10].

It has experimentally been shown that for unsteady processes mesoparticle velocity dispersion does not remain invariable along the average velocity profile $u(t)$ but currently changes. In the steady plastic fronts maximum of dispersion occurs at the middle of front. As for the unsteady shock fronts, behavior of dispersion is not so evident. It may increase along the plastic front up to compressive pulse plateau. Mesostructure analysis of specimens after shock loading shows that there exists a correlation between meso-PVD and strain localization processes. In particular, the rotational (vortex) dynamic straining is realized when PVDF is not symmetrical, which results in asymmetry of the stress tensor (2.9) at the mesolevel, i.e. in nucleating the couple stresses. In distinction from the quasistatic conditions, dynamic couple stresses arise not only due to long-range stress fields of dislocation charges but also due to asymmetry of mesoparticle velocity distribution. Dynamic couple stresses turn out to be sufficiently high to cause the rotational (vortical) motion of medium.

Note by the way, that principle of measuring the meso-PVD developed in [9,10] is based on the assumption that velocity distribution function is equilibrium, and hence has a symmetrical (maxwellian) shape. This proves to be valid only for the steady shock fronts. In general case of unsteady fronts the technique developed in [9,10] is not valid. This technique has been developed in [9]. In unsteady shock front an additional characteristic of mesostructure behavior appears, which is related to the phenomenon of the so-called "fluctuative decay" of shock waves in a structure non-uniform medium. Developed in [9] experimental technique allows to measure particle velocity dispersion and free surface velocity decay at the plateau of compressive pulse. These values prove to be related to each other in a simple way.

Consider that approach in details since it is thought to be of great importance for understanding the coupling between kinetics of elementary carriers of deformation at the mesolevel and kind of kinematical mechanism of dynamic straining and fracture. In accordance with classification suggested by G. E. Duvall [11] there exists three kinds of the wave decay:

i) geometrical decay;
ii) hydrodynamic decay and
iii) "maxwellian" decay.

The first kind of decay relates to space geometry of shock wave. For the spherical wave decay is proportional to $1/r^2$, for the cylindrical wave decay is proportional to $1/r$ and for the plane wave decay does not depends on the propagation distance.

Hydrodynamic kind of decay results from the circumstance that back front of compressive pulse propagates with the higher velocity than the first front because the former moves in the material compressed by the first shock front. For the short three-angle pulses this results in "cutting" upper part of compressive pulse.

Lastly, "maxwellian decay" results from dissipative processes in shock loaded medium.

Besides the enumerated kinds of wave decay, which can exists in steady processes, in unsteady situation an additional kind of wave decay appears, which is stipulated by non-uniform character of the particle motions - the so-called "fluctuative decay". Presented above estimate shows that space scale of structure non-uniformity during the shock wave propagation attributes to mesolevel. The most typical feature of mesolevel is a space and charge heterogenization of dislocation on the distances of the order of their free run (see Fig. 1.3). Mesovolumes

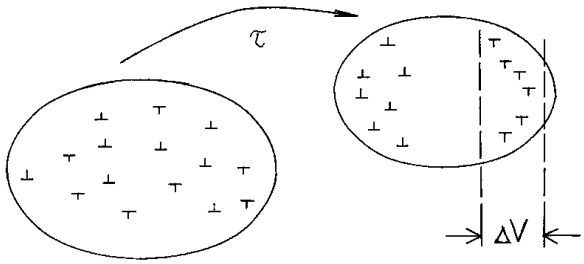


**Fig.1.3.** Nucleation of mesovolumes resulting from polarization of dislocation structure.

$\Delta V$ with polarized dislocation structure can be considered as a quasiparticles with effective charge $q = \Delta r\, \Delta V$ which has a higher radius of interaction as compared to initial state of dislocation structure. Similar to charge particles in plasma, ensemble of mesoparticles can also be characterized by the long-range interaction. That kind of interaction supposes that instead of rear strong interactions between individual particles, a numerous weak interactions happen simultaneously, so that interaction process can be considered as a collective phenomenon. This is an essentially stochastic process, which allows the statistical approach to be used to describe dynamic plasticity at the mesolevel.

Fluctuative braking for individual particle in plasma has been derived by J. Hubburd [12]. It has been shown that trajectory of probe particle in plasma is stochastic and the particle suffers a braking which is proportional to gradient of the velocity dispersion in the velocity space.

One of fundamental equations in stochastic process describing the motion of particles with non-local correlations is known to be the Fokker-Plank equation.

$$\frac{Df}{Dt} = -\frac{\partial}{\partial v}\left[D_1 f(\boldsymbol{v},t)\right] + \frac{1}{2}\frac{\partial^2}{\partial v^2}\left[D_2 f(\boldsymbol{v},t)\right]. \qquad (2.13)$$

Here $f$ ($\boldsymbol{v}$, $t$) is the particle velocity distribution function or probability density. Diffusion coefficients $D_1$ and $D_2$ characterize a change of the particle velocity distribution function due to random interactions of mesoparticles with each other. The first diffusion coefficient $D_1 = d\langle \Delta v \rangle / dt$, or dynamic friction coefficient, characterizes a rate of change of mean velocity due to mutual interactions of mesoparticles. Here $\langle \Delta v \rangle$ is the change of mean particle velocity owing to these interactions. Thus, the value $D_1$ has a sense of deceleration and being multiplied by particle mass defines the value of

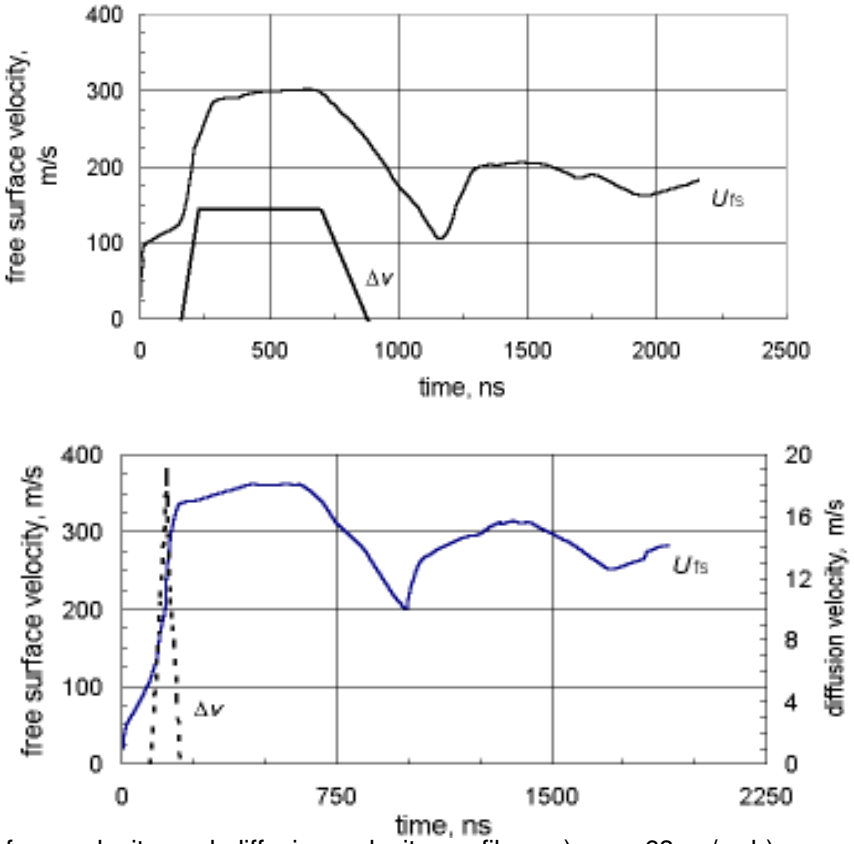


**Fig.1.4.** Free surface velocity and diffusion velocity profiles: a) $u$ = 68 m/s, b) $u$ = 0.

fluctuative friction force directed opposite to the driving force. As a matter of fact, this value defines an additional kind of decay which can be classified as a “fluctuative braking” of particle or “fluctuative decay”. It disappears when the particle velocity dispersion becomes negligible.

The second diffusion coefficient in the Fokker-Plank equation $D_2 = \left\langle \frac{d}{dt}(\Delta v \Delta v) \right\rangle$ defines the rate of change of the mesoparticle velocity dispersion. In case of non-local correlations of particles there exists the following relation between diffusion coefficients [12]:

$$D_1 = \frac{1}{2}\frac{dD_2}{dv}. \qquad (2.14)$$

It is seen from (2.14) that dynamic friction coefficient, and hence the value of the fluctuative friction, depends on the rate of change of the second diffusion coefficient in the velocity space. This conclusion is of great importance for understanding the nature of fluctuative decay not only in case of individual particle having a random trajectory. In case of flow of totality of particles we also deal with braking of flow, i.e., with the fluctuative decay for the mean particle velocity. Analog of equation (2.14) for this case has recently been derived on the basis of the so-called non-local hydrodynamic approach [13].

In case of plastic flow the value $D_1$ in (2.14) defines a current value of the mean deceleration of particle flux. In order to obtain the total decrease of the mean particle velocity due to fluctuative decay it is necessary to integrate over the duration of a process. For example, total decrease of mean particle velocity (decay of mean velocity at the plateau of compressive pulse) for rise-time $\tau$ of shock front can be found as follows:

$$\delta v = \int_0^{\tau} D_1 dt. \qquad (2.15)$$

Consider now typical examples of the dispersion behavior during dynamic deformation of plane steel targets. In Fig.1.4 a,b time-resolved free surface profiles and dispersion histories for viscous high-strength 30XH4M steel and stainless steel 12X18H10T are presented. The first free surface profile has been obtained at the impact velocity of 369 m/s. It is seen from Fig. 1.4a that pick value of the free surface velocity equals ≈ 300 m/s, i.e. the free surface velocity decay equals 69 m/s.

In Fig.1.4b analogous couple of dependencies is provided for the stainless steel 12X18H10T target loaded at the impact velocity of 366.5 m/s. Free surface velocity in this case turns out to be 365 m/s, which is closely to impact velocity. This means that fluctuative decay of mean velocity for that material is very small or negligible at all. At the same time behavior of the diffusion velocity here differs from previous case very strong. Diffusion velocity for that test achieves a value of 20 m/s in the middle of plastic front of compressive pulse. Use of the equations (2.14) and (2.15) for that case results in zero value of fluctuative decay because dynamic friction coefficient has time to change its sign on opposite in the middle of plastic front, so that time integration over the plastic front gives zero value of the velocity decay.

### 2.2. Stochastic Approach for Change of Strain Kinematics

Aforedescribed phenomenon of decrease of the flux velocity due to particle velocity distribution can also be described in terms of structural phase transition initiated by the noise, the role of noise plays the velocity distribution of mesoparticles during the shock wave propagation. The situation appears to be closely corresponded to the well-known population genetic model under conditions of external noise [14].

$$\frac{d}{dt}\boldsymbol{X}(t) = \lambda(t)\boldsymbol{X}(t) - \boldsymbol{X}^2(t). \qquad (2.16)$$

In our case dynamic variable $\boldsymbol{X}(t)$ has the sense of mean particle velocity $u(t)$ defined above via the particle velocity distribution function $f(r,v,t)$. Parameter $\lambda(t)$ characterizes an influence of external conditions on the considered nonlinear system. It consists of two parts one of which $\lambda_0$ is regular while another $\xi$ is a noise:

$$\lambda = \lambda_0 + D\xi. \qquad (2.17)$$

Here $D$ is the intensity of noise. Detail analysis in [14] shows that probability density for dynamic variable $\boldsymbol{X}(t)$ has two distinctive maximums, one of which corresponds to zero value of dynamic variable $\boldsymbol{X}(t) = 0$ and another - to some positive value $\boldsymbol{X} > 0$, the zero value corresponds to large values of noise intensity $D$.

The same may be seen for the wave propagation in non-uniform medium. Consider this situation in details accepting that mesoparticles can be considered as dislocations having a summary Burgers-vector $B$ for polarized dislocation structure shown in Fig.1.3. In this case one can use the Orowan equation for plastic deformation:

$$\varepsilon = B\rho l_d. \qquad (2.18)$$

Here $\rho$ is the mesoparticle density and $l_d$ is their run. Differentiating this equation on time gives:

$$\frac{d\varepsilon}{dt} = Bl_d\frac{d\rho}{dt} + B\rho\frac{dl_d}{dt}. \qquad (2.19)$$

In accordance with dislocation dynamics the time derivative of dislocation density ($d\rho/dt$) can be written as follows [15]:

$$\frac{d\rho}{dt} = \alpha\rho - \beta\rho^2. \qquad (2.20)$$

Here $\alpha$ characterizes the intensity of nucleation of mesoparticles in the process of polarization of dislocation structure and $\beta$ is the coefficient which takes into account their attrition and/or annihilation. On the other hand, on definition, deformation can be expressed in the form:

$$\varepsilon = \frac{dU}{dX} = \left(\frac{dU}{dt}\right)/\left(\frac{dX}{dt}\right) = \frac{v}{C_p}, \qquad (2.21)$$

where $U$ is the displacement, $v$ is the particle velocity and $C_p$ is the plastic wave speed. For the steady plastic fronts $C_p$ = const and strain rate equals:

$$\frac{d\varepsilon}{dt} = \frac{1}{C_p}\frac{dv}{dt}. \qquad (2.22)$$

By using (2.18) – (2.22) one obtains:

$$\frac{dv}{dt} = C_pB\frac{dl_d}{dt} + \alpha v - \frac{\beta}{Bl_dC_p}v^2. \qquad (2.23)$$

If one accepts that mesoparticle run is invariable (equal, for instance, to grain size) equation (2.23) transforms into equation similar to equation (2.16) for genetic model:

$$\frac{dv}{dt} = \alpha v - \chi v^2, \qquad (2.24)$$

where $\chi=\beta/Bl_dC_p$. In that equation $(\alpha)^{-1}$ has the sense of time of macroscopic evolution of non-linear system while $(\chi)^{-1}$ is the distance over what annihilation of mesoparticles occurs. In order to change over to proper stochastic equation one should take parameter $\alpha$ consisting of regular and noise parts: $\alpha = \alpha_0 + D\xi(t)$. The sense of noise intensity $D$ will be clear

below. The stochastic equation corresponding to deterministic equation (2.24) has the form [14]:

$$dv = (\alpha v - \chi v^2)dt + D^2 v \bullet dW. \qquad (2.25)$$

Solution to that equation is known to seek in the form of probability density. Its time evolution is described by the proper Fokker-Plank equation corresponding to stochastic equation (2.25). In the Sctratonovich interpretation that equation can be written as follows:

$$\frac{d}{dt}f(v,t) = -\frac{\partial}{\partial v}\left[\left(\alpha v - \chi v^2 + \frac{D^2}{2}v\right)f(v,t)\right] + \frac{D^2}{2}\frac{\partial^2}{\partial v^2}\left[v^2 f(v,t)\right]. \qquad (2.26)$$

Stationary solution to this equation has the form:

$$f(\boldsymbol{v}) = N^{\left(\frac{2\alpha}{D^2}-1\right)}\exp\left(-\frac{2\alpha}{D^2}\right), \qquad (2.27)$$

where

$$N^{-1} = \left[\frac{2}{D^2}\right]^{\left(\frac{2\alpha}{D}-1\right)}\Gamma\left(\frac{D^2}{2\alpha}\right).$$

Extremes of probability density define the position of phase transitions on the velocity axis. They can be determined from the equation:

$$\alpha v - \chi v^2 - \frac{D^2}{2}v = 0, \qquad (2.28)$$

which has two roots:

$$1)\ v = 0; \quad 2)\ v = \frac{1}{\chi}\left(\alpha - \frac{D^2}{2}\right). \qquad (2.29)$$

The first root means that probability density has extreme at zero average velocity $v = 0$.

The second root corresponds to phase transition under condition of $\alpha = D^2/2$, which can be considered as criterion for noise-induced structural phase transition. When $\alpha > D^2/2$, maximum of probability density is shifted to the right on the velocity axis. Now we are in position to define the physical sense for the noise intensity $D^2/2$. For this purpose we remind that the first item in the right hand side of the Fokker-Plank equation (2.26) includes the diffusion coefficient $D_1$:

$$D_1 = \frac{d}{dt}\langle \Delta v \rangle = \alpha v - \chi v^2 + \frac{D^2}{2}v. \qquad (2.30)$$

And the second diffusion coefficient

$$D_2 = \left\langle \frac{d}{dt}(\Delta v \Delta v)\right\rangle = D^2 v^2. \qquad (2.31)$$

Equation (2.30) can be rewritten as follows:

$$\frac{D_1}{v} = \alpha - \chi v + \frac{D^2}{2}.$$

When $\alpha = \chi v$,

$$\frac{D^2}{2} = \frac{D_1}{v} \quad \text{or} \quad \frac{D^2}{2} = \frac{1}{v}\frac{d\langle \Delta v\rangle}{dt}. \qquad (2.32)$$

Resonance condition $\alpha = \chi v$ or $\frac{1}{\chi} = \frac{v}{\alpha}$ means that macroscopic space scale of evolution of the considered system $l_{macro} = \frac{v}{\alpha} = \tau_{macro} v$ coincides with the value $\frac{Bl_d C_p}{\beta}$, which equals to the free run of mesoparticles before their annihilation or locking. Right hand side of (2.32) can be rewritten in the form:

$$\frac{1}{v}\frac{d\langle \Delta v\rangle}{dt} = \frac{d}{dt}\left\langle \frac{\Delta v}{v}\right\rangle \qquad (2.33)$$

under condition of

$$\frac{d\langle \Delta v\rangle}{dv} >> \frac{\langle \Delta v\rangle}{v}. \qquad (2.34)$$

Indeed,

$$\frac{d}{dt}\left\langle \frac{\Delta v}{v}\right\rangle = \frac{1}{v}\frac{d\langle \Delta v\rangle}{dt} + \frac{dv}{dt}\langle \Delta v\rangle =$$

$$\frac{1}{v}\frac{dv}{dt}\left[\frac{\frac{d\langle \Delta v\rangle}{dt}}{\frac{dv}{dt}} + \frac{\langle \Delta v\rangle}{v}\right] =$$

$$\frac{1}{v}\frac{dv}{dt}\left[\frac{d\langle \Delta v\rangle}{dv} + \frac{\langle \Delta v\rangle}{v}\right] \cong \frac{1}{v}\frac{d\langle \Delta v\rangle}{dt}.$$

In our case the condition (2.34) means that the current rate of change of diffusion velocity is higher than its total change over the plastic wave front. Eq. (2.31) under the condition (2.34) can be written as follows:

$$D^2 = \frac{D_2}{v^2} \cong \left\langle \frac{d}{dt}\left(\frac{\Delta v \Delta v}{v^2}\right)\right\rangle. \qquad (2.35)$$

From (2.32) and (2.35) one obtains:

$$\frac{d}{dt}\left\langle \frac{\Delta v}{v} \right\rangle = \frac{1}{2}\left\langle \frac{d}{dt}\left( \frac{\Delta v \Delta v}{v^2} \right) \right\rangle. \qquad (2.36)$$

This means that under resonance condition $\alpha = \chi v$ the rate of change of the diffusion velocity $\langle \Delta v \rangle$ normalized by the current value of the velocity $v$ equals the half – rate of change of the velocity dispersion normalized by the current velocity square $v^2$.

The condition for phase transition $\alpha = D^2/2$ is:

$$\alpha = \frac{d\zeta^2}{dt} \qquad (2.37)$$

or

$$\frac{\alpha}{\varsigma} = \frac{d\varsigma}{dt}, \qquad (2.38)$$

where $\varsigma = \left\langle \frac{\Delta v}{v} \right\rangle$. Under strain rates where $\alpha << d\zeta^2/dt$, maximum of probability density corresponds to particle velocity $v = 0$. If, however, particle velocity dispersion changes slowly, one has an opposite situation when $\alpha >> d\zeta^2/dt$. In this case a flux motion of mesoparticles takes place with a non-zero average velocity in the wave propagation direction.

Presented analysis shows that in dynamic processes related to structural phase transitions the most important characteristic becomes not only the mesoparticle velocity dispersion but the rate of its change. The above analysis also shows that dynamically deformed solid can display different behavior of elementary carriers of deformation at the mesolevel. The first one corresponds to situation when the mean particle velocity at the plastic front equals zero. The second regime corresponds to opposite situation, when all the mesoparticles move with the identical velocities in the wave propagation direction. Transition between these states can be treated as structure phase transition, realization of which is determined by the by the rate of change of the particle velocity dispersion.

Equation (2.38) can be written in the form:

$$\frac{\frac{v}{\langle \Delta v \rangle}}{\tau} = \frac{d\left( \frac{\langle \Delta v \rangle}{v} \right)}{dt}, \qquad (2.39)$$

where $\tau = 1/\alpha$ is the time of macroscopic evolution of the considered system. In this case inequality

$$\frac{\frac{v}{\langle \Delta v \rangle}}{\tau} << \frac{d\left( \frac{\langle \Delta v \rangle}{v} \right)}{dt}, \qquad (2.40)$$

means that the rate of grow of the relative mean particle velocity (i.e., normalized by the diffusion velocity) for the full duration of the process (in our case rise-time of plastic front) is more smaller than the current rate of grow of the diffusion velocity normalized by the average velocity over the front. In other words, change of the particle velocity dispersion happens more quickly than the change of the average particle velocity. In the opposite case, when

$$\frac{\frac{v}{\langle \Delta v \rangle}}{\tau} >> \frac{d\left( \frac{\langle \Delta v \rangle}{v} \right)}{dt}, \qquad (2.41)$$

the change of the velocity dispersion occurs slower as compared to the average particle velocity. The first case corresponds to the situation when all additional kinetic energy supplied to medium immediately transforms into chaotic motion of mesostructure, so the average particle velocity doesn't change. In the second case, on the contrary, additional energy supplied to medium results in increase of the flux motion of mesostructure.

## 3. EXPERIMENTAL STUDY OF STRENGTH PROPERTIES OF STEELS

### 3.1. Experimental Approach.

The experiments on shock loading of plane targets were performed by using a light gas gun facility of 37 mm bore diameter. All the targets were 52 mm in diameter, impactor has a glass shape of 28 mm in diameter, 2 mm thick and 8 mm height of walls. Impactor plates of the same material as the target are mounted at the front of the projectile, which is accelerated to the impact velocity of 50 - 600 m/s. Thickness of targets and impactor were adjusted to provide a spallation at every shock provided the criterion for spallation is fulfilled.

Impactor velocity was determined at each test by measuring the time interval of projectile flying between two transverse laser beams of fixed spacing.

The time-resolved free surface velocity profiles were recorded using a two-channel velocity interferometer [9]. This technique allows, besides the mean particle velocity, to determine also an additional characteristic of the mesoparticle kinetics which characterizes a particle velocity distribution within

**Table 1.** Results of tests for the 1-st set of 40XCHMA steel.

| N | Target thick., mm | Impactor thick., mm | Impactor velocity, m/s | Decay of vel. $\delta v$, m/s | Diffusion vel. $\langle \Delta v_1 \rangle$, m/s | Pull-back velocity $W$, m/s |
|---|---|---|---|---|---|---|
| 1 | 5.35 | 1.98 | 211 | 16.1 | 0 | 166.1 |
| 2 | 5.30 | 2.00 | 215 | 14.3 | 0 | 168.7 |
| 3 | 5.36 | 1.96 | 2.90 | 29.6 | 7.6 | 194.9 |
| 4 | 5.06 | 2.00 | 307 | 15.3 | 8.5 | 183.9 |
| 5 | 5.59 | 1.95 | 309 | 29.6 | 0 | 180.5 |
| 6 | 5.25 | 1.98 | 329 | 22.3 | 10.0 | 195.1 |
| 7 | 5.26 | 2.15 | 356 | 20.3 | 11.7 | 179.2 |
| 8 | 5.2 | 1.99 | 379 | 35.2 | 16.1 | 200.9 |
| 9 | 5.35 | 1.99 | 405 | 21.3 | 21.5 | 214.5 |
| 10 | 4.83 | 1.97 | 437 | 30.0 | 19.2 | 200.3 |

the laser beam cross-section. The term “mesoparticle kinetics” herein has the same sense as in the physical kinetics of fluid and gas, i.e. such behavior of the particles which can be characterized by some distribution in the velocity space. The width of that distribution, or the square root of the particle velocity dispersion, has been defined in Section 2 as a “diffusion velocity” of mesostructure. It’s considered as a very important quantitative characteristic of mesoparticle kinetics. Determination of the latter is grounded on the measurement of the interference signal contrast. The process of reflecting of the primary monochromatic laser radiation from target may be represented as a generation of a totality of micro-beams every of which interacts with one concrete mesoparticle of the target surface. As a result of that interaction and due to the fact that all the particles have different velocities, the elementary micro-beams acquire different Doppler shifts of laser radiation. This leads to decreasing the degree of monochromaticity of the summary radiation, which is equivalent to widening of its spectrum. Analysis of the phenomenon has previously been performed in [9].

### 3.2. Characteristics of Materials and Results of Tests

1) 40XCHMA steel.

This is complex alloyed steel of sufficiently high hardness (HRc 55) commonly used as armor steel. Spall-strength characteristics for the 40XCHMA steel were studied for two sets of targets – 5 mm and 2mm thickness. This was done to check an influence of steadiness of shock wave on dynamic strength of this steel.

a). Results of shock tests for the 5 mm targets are presented in Table 1 and Table 2. In Table 1 the second column is the thickness of target, the third

**Table 2**. Data of calculation of stress-strain diagram for 40XCHMA steel.

| N | Target thick., mm | Impact thick., mm | Imp. vel., m/s | Maximum vel. $U_{max}$, m/s | HEL $U_{HEL}$, m/s | Plastic vel. $C_p$, km/s | Stress $\sigma$, GPa | Strain $\varepsilon$ $10^{-2}$ |
|---|---|---|---|---|---|---|---|---|
| 1 | 5.35 | 1.98 | 211 | 196.1 | 113 | 5.52 | 4.34 | 1.69 |
| 2 | 5.30 | 2.66 | 2.15 | 202.8 | 112.5 | 5.5 | 4.75 | 1.757 |
| 3 | 5.36 | 1.96 | 290 | 261 | 125 | 5.32 | 5.78 | 2.55 |
| 4 | 5.06 | 2.00 | 307 | 2.91.3 | 131.2 | 5.34 | 6.44 | 2.59 |
| 5 | 5.59 | 1.95 | 309 | 279.8 | 125 | 5.29 | 6.157 | 2.5 |
| 6 | 5.25 | 1.98 | 329 | 297 | 131.3 | 5.29 | 6.54 | 2.66 |
| 7 | 5.26 | 2.15 | 356 | 336.5 | 128 | 5.21 | 7.28 | 3.07 |
| 8 | 5.20 | 1.99 | 379 | 345 | 125 | 5.29 | 7.51 | 3.12 |
| 9 | 5.35 | 1.99 | 405 | 383.3 | 107.4 | 5.34 | 8.313 | 3.48 |
| 10 | 4.83 | 1.97 | 437 | 408.9 | 136.3 | 5.32 | 8.9 | 3.7 |

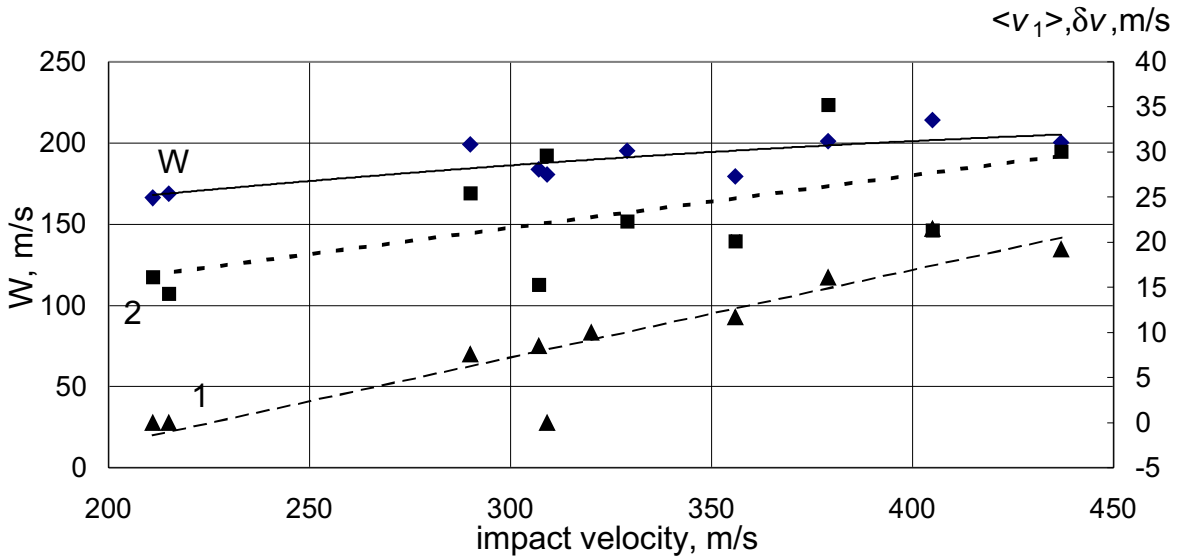


**Fig.3.1.** Dependencies of pull-back velocity *W,* diffusion velocity at the mesolevel-1$\langle \Delta v_1 \rangle$ (1), velocity decay $\delta v_2$ (2) on the impact velocity (40XCHMA steel).

columns is the thickness of impactor, column fourth is the impact velocity $U_{imp}$. Column fifth is the free surface velocity decay $\delta v$, column sixth is the diffusion velocity at mesolevel-1$\langle \Delta v_1 \rangle$ and seventh column is the pull-back velocity *W*. Dependencies of pull-back velocity *W*, free surface velocity decay $\delta v$ and diffusion velocity at the mesolevel-1$\langle \Delta v_1 \rangle$ on the impact velocity are presented in Fig. 3.1, which shows that $W=f(U_{imp})$, $\langle \Delta v_1 \rangle = f(U_{imp})$ and $\delta v = f(U_{imp})$ monotonously grow with the impact velocity.

In accordance with our approach there are two criteria which influence the spall-strength of material. The first criterion requires that the diffusion velocity at the mesolevel-1 must be equal or greater than diffusion velocity at the mesolevel-2:

$$\langle \Delta v_1 \rangle \geq \langle \Delta v_2 \rangle . \qquad (3.1)$$

In this case local stresses at the meslevel-2 are suppressed by the velocity dispersion at the mesolevel-1. Interference technique permits to measure only the diffusion velocity at the mesolevel-1$\langle \Delta v_1 \rangle$. In order to determine the diffusion velocity at the mesolevel-2 we plot a dependence of the free surface velocity decay $\delta v$ on the impact velocity together with deviations of velocity separately (see Fig. 3.2). These deviations can be accepted as current values of the diffusion velocity at the mesolevel-2. In Fig. 3.3 dependencies for diffusion velocities are plotted together with pull-back velocity. Intersection of diffusion velocities happens at the impact velocity of 270 m/s (point A). One can see that practically within overall range of impact velocities the first optimum condition for dynamic deformation and fracture (3.1) is fulfilled and pull-back velocity shows monotonous increase.

The second criterion for optimum dynamic deformation and fracture requires that diffusion velocity at the mesolevel-1 must be equal or greater than the free surface velocity decay.

$$\langle \Delta v_1 \rangle \geq \delta v. \qquad (3.2)$$

In Fig. 3.1 these dependencies have different inclination. This means that these dependencies intersect each other at higher impact velocity. In order to find their intersection in Fig. 3.4 these curves are plotted in another scale. It's seen that the intersection of the curves happens at the impact velocity of 695 m/s and would correspond to the pull-back velocity of 250 m/s. Thus, within the impact velocities range of 211 – 437 m/s this steel hasn't optimum spall-strength characteristics.

Normal stress and strain at the plastic front are calculated by using the formulae:

$$\sigma = 0.5\rho\left[U_{max}C_p^l + U_{HEL}(C_l - C_p^l)\right], \qquad (3.3)$$

$$\varepsilon = 0.5\left[\frac{U_{HEL}}{C_l} + \frac{U_{max} - U_{HEL}}{C_p^l}\right]. \qquad (3.4)$$

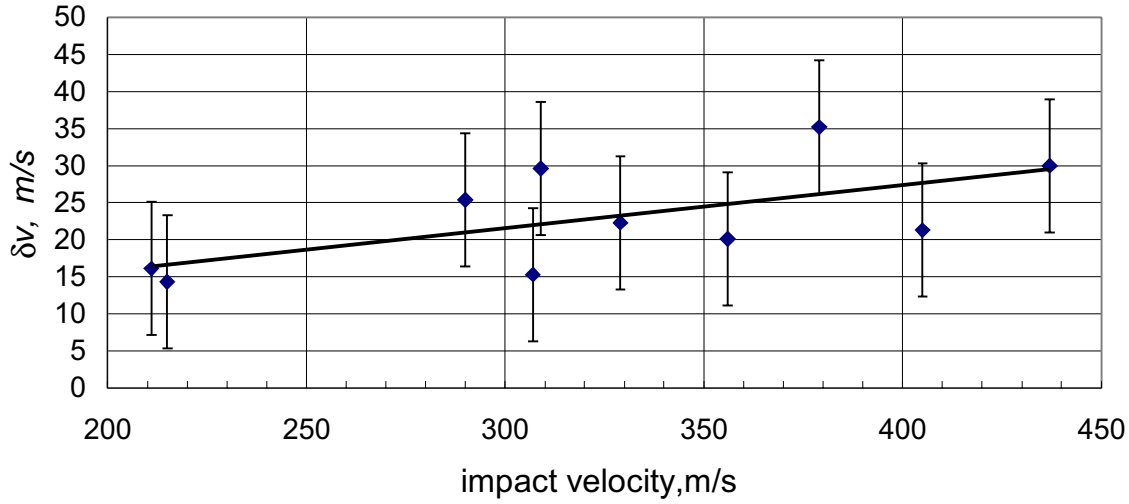


**Fig.3.2.** Dependence of the defect of the free surface velocity on the impact velocity (1-st set of 40XCHMA steel).

$$C_p^1 = \frac{h_t}{h_t(C_l + \Delta t_1)}. \qquad (3.5)$$

Here $h_t$ is the target thickness, $C_l$ is the longitudinal sound velocity in steel ($C_l$=5.95 km/s), $C_p^1$ is the plastic front velocity determined on the basis of measuring a delay $\Delta t_1$ of plastic front relatively elastic precursor. In Table 2 sixth column presents the free surface velocity at the elastic precursor, seventh column is the average velocity of load plastic front $C_p^1$, eighth column is the stress value at the plateau of compressive pulse and ninth column gives the strain.

Stress-strain diagram for the 40XCHMA steel is presented in Fig. 3.5.

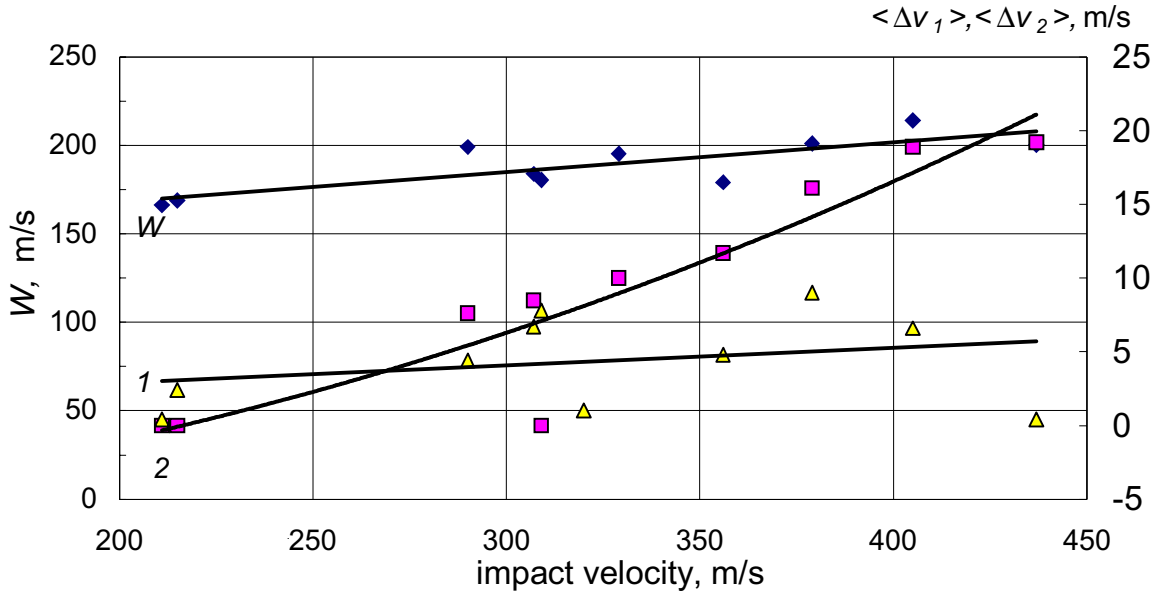


**Fig.3.3.** Pull-back velocity *W*, diffusion velocity at the mesolevel-1$\langle \Delta v_1 \rangle$ (1) and mesolevel-2$\langle \Delta v_2 \rangle$ (2) on the impact velocity (1-st set of 40XCHMA steel).

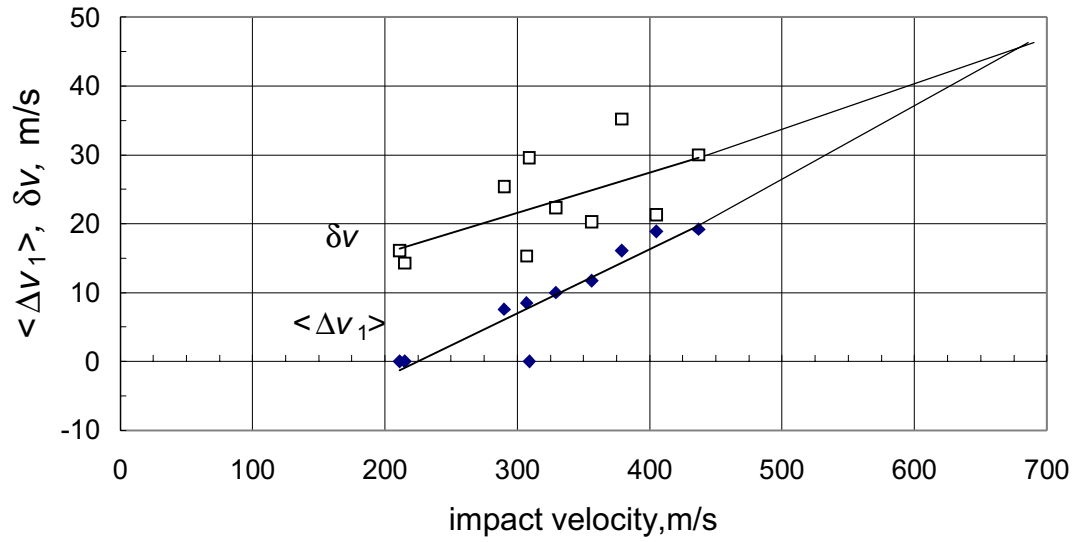


**Fig.3.4.** Dependence of the diffusion velocity $\langle \Delta v_1 \rangle$ and velocity decay $\delta v$ on the impact velocity (1-st set of 40XCHMA steel).

b). Results of shock test of 2 mm steel targets are provided in Table 3. In Fig. 3.6 we present the dependencies $W = f(U_{imp})$, $\langle \Delta v_1 \rangle = f(U_{imp})$, $\langle \Delta v_2 \rangle = f(U_{imp})$ and $\delta v = f(U_{imp})$ altogether. To draw the dependence $\langle \Delta v_2 \rangle = f(U_{imp})$ in Fig. 3.7 dependence $\delta v = f(U_{imp})$ is presented separately. In Fig. 3.8 dependencies $\langle \Delta v_1 \rangle = f(U_{imp})$ and $\langle \Delta v_2 \rangle = f(U_{imp})$ are presented together. One can see that dependence $\langle \Delta v_1 \rangle = f(U_{imp})$ lies above $\langle \Delta v_2 \rangle = f(U_{imp})$, which means that criterion (3.1) is satisfied. As for the second criterion (3.2), it's satisfied only below the impact velocity of 495 m/s after what velocity decay $\delta v$ remains upward the diffusion velocity. This means that 2 mm targets have optimum spall-strength only at the impact velocities beneath 495 m/s. Its value is approximately equaled to the spall-strength (~ 250 m/s), which is expected for the 5 mm targets if the optimum kinetic characteristics are provided.

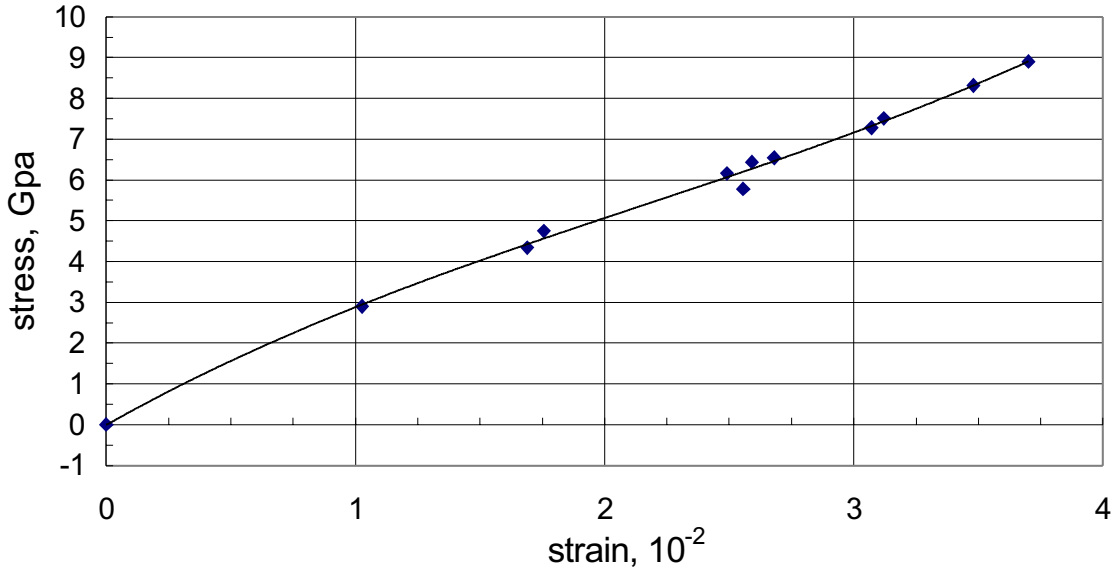


**Fig.3.5.** Stress-strain diagram for the 40XCHMA steel.

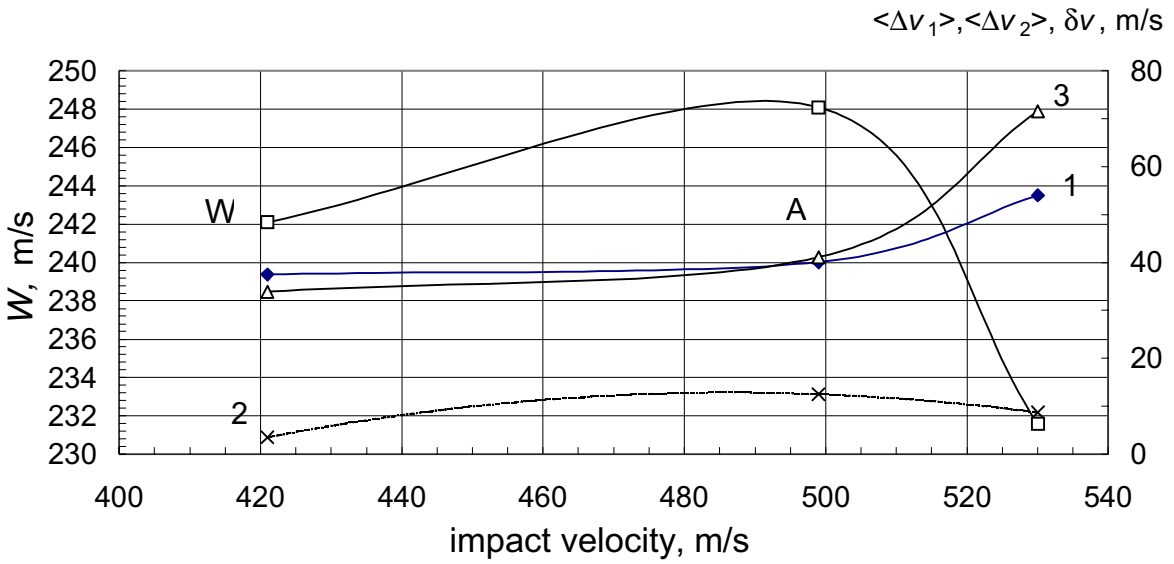


**Fig.3.6.** Dependencies of pull-back velocity $W$, diffusion velocity at the mesolevel-1 $\langle \Delta v_1 \rangle$ (1), mesolevel-2 (2) and velocity decay $\delta v$ on the impact velocity (3) (2-nd set of 40XCHMA steel).

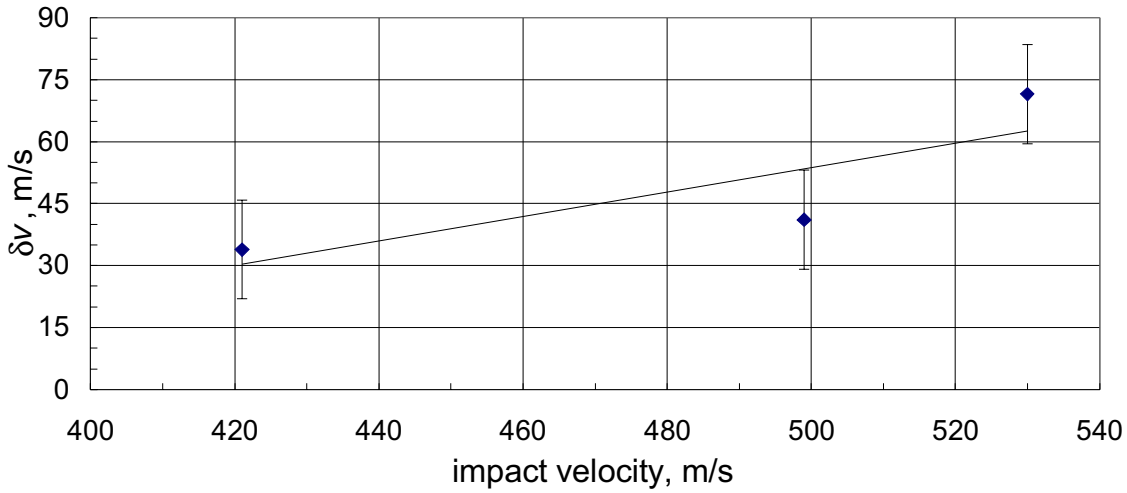


**Fig.3.7.** Decay of the free surface velocity versus impact velocity (2-nd set of 40XCHMA steel).

**Table 3.** Results of tests for 2-nd set of 40XCHMA steel.

| N | Target thickn., mm | Impactor thickn., mm | Impactor velocity, m/s | Decay of vel., $\delta v$, m/s | Diffusion velocity, $\langle \Delta v_1 \rangle$, m/s | Pull-back velocity, $W$, m/s |
|---|---|---|---|---|---|---|
| 1 | 2.01 | 1.00 | 421 | 33.9 | 35.2 | 242.1 |
| 2 | 1.99 | 0.99 | 499 | 41.1 | 40.1 | 248.1 |
| 3 | 1.99 | 1.00 | 530 | 71.5 | 54 | 231.6 |

**Table 4.** Results of test for 1-st set of 38ХН3МФА steel.

| N | Target thickn., mm | Impactor thickn., mm | Impact vel. $U_{imp}$, m/s | Decay vel. $\delta v$, m/s | Diffusion velocity, $\langle \Delta v_1 \rangle$, m/s | Pull-back velocity, $W$, m/s |
|---|---|---|---|---|---|---|
| 369 | 5.68 | 2.06 | 200.9 | 19.6 | – | – |
| 370 | 5.68 | 2.04 | 239.3 | 18.1 | 9.7 | 169.4 |
| 368 | 5.68 | 2.10 | 263.1 | 15.3 | 8.4 | 180.7 |
| 367 | 5.68 | 2.10 | 306.4 | 23.9 | 13.6 | 180.4 |
| 366 | 5.68 | 2.09 | 346.7 | 25.5 | 15.7 | 187.1 |
| 371 | 5.65 | 1.99 | 349 | 12 | 11.5 | 189.8 |
| 372 | 5.62 | 2.02 | 373.5 | 9.6 | 16.1 | 193.3 |
| 365 | 5.68 | 2.09 | 404.3 | 13.8 | 21.3 | 203.3 |

2). 38ХН3МФА steel.

This is complex-alloyed Cr-Ni-Mo steel. Under quasistatic conditions this steel has a high plasticity and strength. Presence of Ni results in increase of viscosity of the steel while the presence of Mo provides its high heat resistance. So this steel can be used up to temperature of 400-500 °C. This steel is used for manufacturing the executive details of turbines and compressors (forging of driving shafts and whole-forged rotors of reducers). Two sets of targets have been tested. The first set has been made from the material as supplied and the second – from the same steel after thermal treatment providing a homogenization of structure. As a result, the first kind of steel has obvious features of texture whereas the structure of the second steel is characterized by homogeneous equal-axis grain structure.

a). The first set of 38ХН3МФА steel targets (HRC 39). Results of tests are provided in Table 4. Dependencies of pull-back velocity, the free surface velocity decay and diffusion velocity at the mesolevel-1 and mesolevel-2 on the impact velocity are presented in Fig. 3.9.

One can see that pull-back velocity grows in parallel to the diffusion velocity up to impact velocity of 350 m/s after what it increases. Just that impact velocity corresponds to point where curves $\delta v = f(U_{imp})$

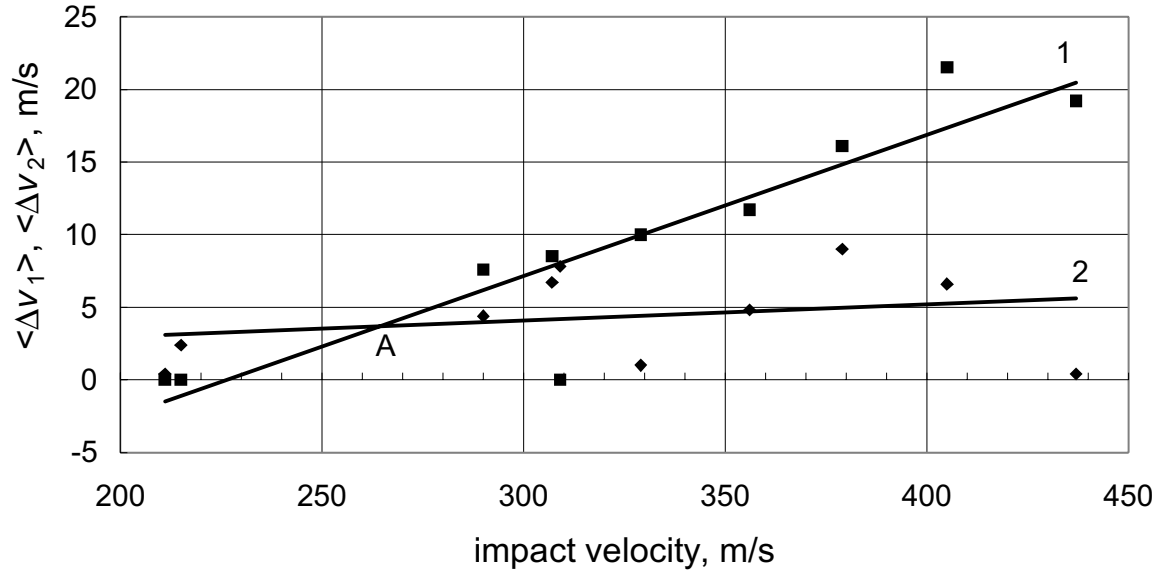


**Fig.3.8.** Diffusion velocity at the mesolevel-1 $\langle \Delta v_1 \rangle$ (1), mesolevel-2 $\langle \Delta v_2 \rangle$ (2) versus impact velocity (2-nd set of 40ХСНМА steel).

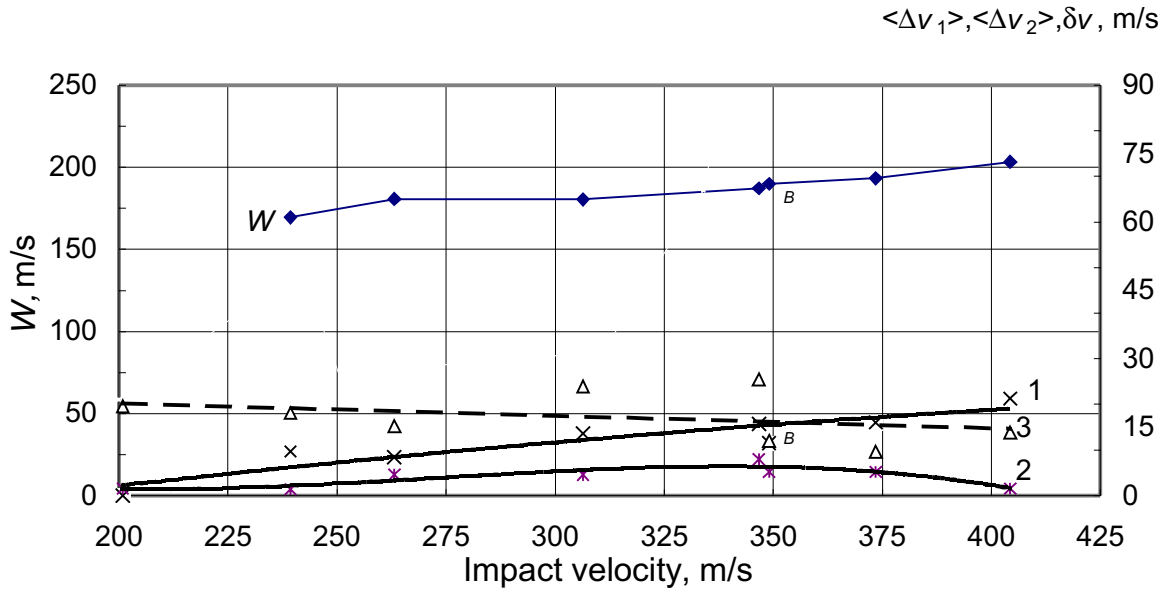


**Fig.3.9.** Pull-back velocity *W*, diffusion velocity at the mesolevel-1 $\langle \Delta v_1 \rangle$ (1), mesolevel-2 $\langle \Delta v_2 \rangle$ (2), and velocity decay δv (3) versus impact velocity (1-st set of 38ХН3МФА steel).

and $\langle \Delta v_1 \rangle = f(U_{imp})$ intersect and diffusion velocity becomes higher than the velocity decay, so criterion (3.2) is fulfiled. This situation confirms our previous assertion that particle velocity dispersion characterizes an ability of material to relax internal stresses and thereby to increase macroscopic dynamic strength of steel. On the other hand, value of the free surface velocity decay results from pumping over a shock-wave energy from level meso-1 to level meso-2. When the free surface velocity decay increases, this means that instead of relaxation of internal stresses at the mesolevel-1, an accumulation of stresses occurs at the next scale level meso-2, which results in large-scale fragmentation of material and fracture. On the contrary, if the free surface velocity decay at the mesolevel-2 is smaller than the diffusion velocity at the mesolevel-1, accumulation of internal stresses at the level meso-2 is suppressed. In this case the local stresses are resolved and large-scale fragmentation of material at the mesolevel-2 isn't initiated, which results in increase of its dynamic strength. Just that situation happens after impact velocity of 350 m/s.

In Fig. 3.10 the free surface velocity $U_{max}$ as a function of impact velocity is presented separately. In this figure we also present a symmetrical curve

**Table 5.** Results of calculation of stress-strain diagram for the 38ХН3МФА steel.

| N | Target thick., mm | Impact thick., mm | Imp. vel. $U_{imp}$, m/s | Maximum fr. s. vel. $U_{max}$, m/s | HEL vel. $U_{HEL}$, m/s | Plastic vel. $C_p$, km/s | Stress σ, GPa | Strain ε $10^{-2}$ |
|---|---|---|---|---|---|---|---|---|
| 369 | 5.68 | 2.06 | 200.9 | 181.3 | 62 | 5.03 | 3.78 | 1.71 |
| 370 | 5.68 | 2.04 | 239.3 | 221.2 | 58 | 5.01 | 4.53 | 2.12 |
| 368 | 5.68 | 2.10 | 263.1 | 247.8 | 63 | 5.01 | 5.07 | 2.37 |
| 367 | 5.68 | 2.10 | 306.4 | 282.5 | 60 | 5.05 | 5.77 | 2.71 |
| 366 | 5.68 | 2.09 | 346.7 | 321.2 | 57 | 5.03 | 6.51 | 3.11 |
| 371 | 5.65 | 1.99 | 349 | 337 | 62 | 5.01 | 6.81 | 3.27 |
| 372 | 5.62 | 2.02 | 373.5 | 363.9 | 64 | 5.04 | 7.38 | 3.51 |
| 365 | 5.68 | 2.09 | 404.3 | 390.5 | 63 | 5.04 | 7.90 | 3.78 |

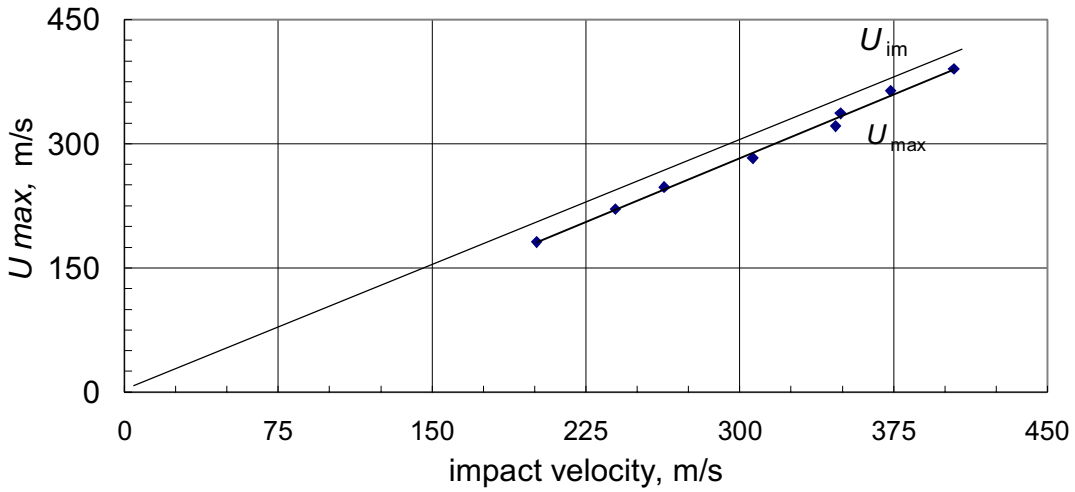


**Fig.3.10.** Pick value of the free surface velocity versus impact velocity (1-st set of 38ХН3МФА steel).

corresponding to the impact velocity (dotted line). One can see that the free surface velocity at the plateau of compressive pulse smaller than the impact velocity approximately by 20 m/s.

In Table 5 the results of calculating stress-strain diagram are provided. The stress-strain diagram for the 38ХН3МФА steel is presented in Fig. 3.11.

In order to check the criterion (3.1) for that steel in Fig. 3.12 we present a dependence of the free surface velocity decay $\delta v$ on the impact velocity. This curve allows to plot the dependence of the diffusion velocity at the mesolevel-2 on the impact velocity. Both dependencies for diffusion velocity at the mesolevel-1 and mesolevel-2 are provided in Fig. 3.13. One can see that diffusion velocity at the mesolevel 2 lies below so the criterion (3.1) is satisfied within overall range of impact velocities. Thus, for the first set of 38ХН3МФА steel both criterion for structure optimization are satisfied after impact velocity 350-375 m/s.

b). The second set of 38Н3МФА steel targets has been subjected to tempering to provide a grain homogenization. Results of testing are provided in Table 6. Dependencies of pull-back velocity *W*, the free surface velocity decay $\delta v$ and diffusion velocity $\langle \Delta v_1 \rangle$ at the mesolevel-1and mesolevel-2 on the impact

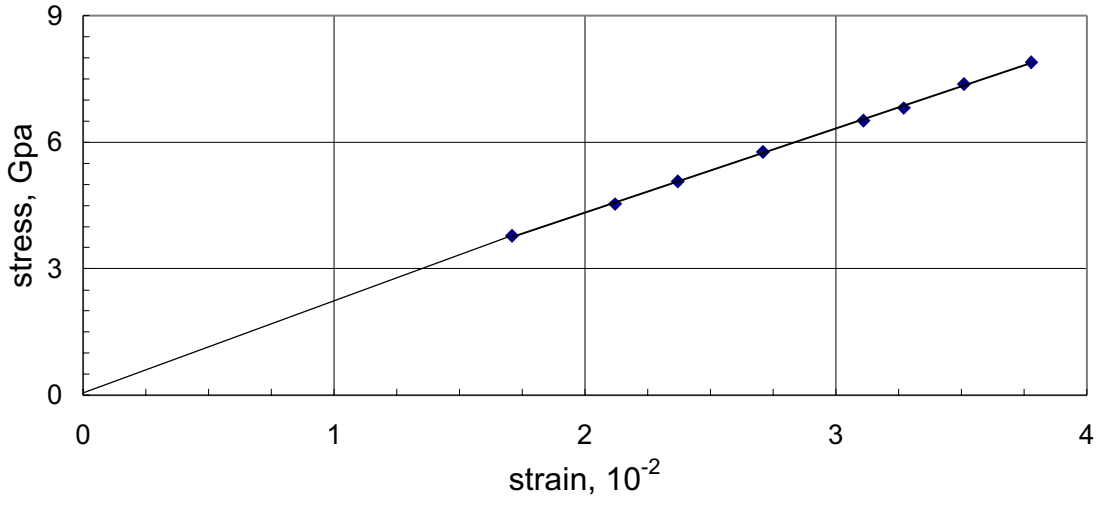


**Fig.3.11.** Stress-strain diagram for the 38ХН3МФА steel.

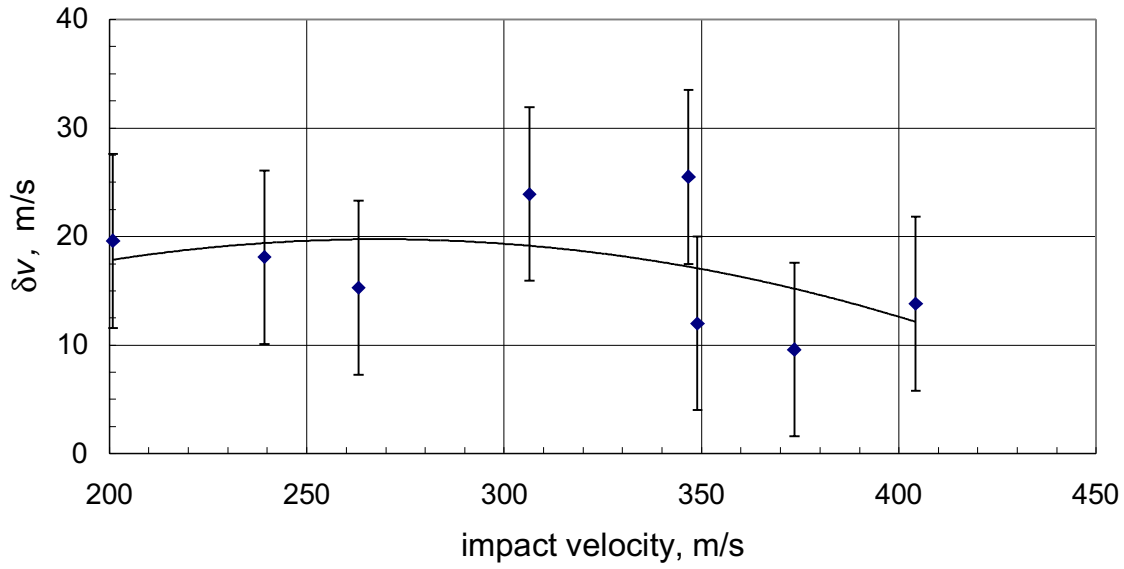


**Fig.3.12.** Defect of the free surface velocity versus impact velocity (1-st set of 38ХН3МФА steel).

velocity are provided in Fig.3.14. This kind of steel reveals a non-monotonous behavior of spall-strength on the strain rate. Dependence $W = f(U_{imp})$ has two turning-points – at impact velocity of ~275 m/s and 310 m/s. To check the criterion (3.1) in Fig. 3.15 the free surface velocity decay versus impact velocity is provided separately. On the basis this dependence a diffusion velocity for the mesolevel-2 $\langle \Delta v_2 \rangle$ is built. Both dependencies for diffusion velocity at the mesolevel-1 and mesolevel-2 are plotted in Fig. 3.16. One can see that diffusion velocity at the mesolevel-1 becomes higher than that at the mesolevel-2 after impact velocity ~275 m/s. Just that velocity corresponds to increase of the spall-strength of steel (see Fig. 3.14).

Maximum pull-back velocity at the impact velocity of ~295 m/s where dependencies of the free surface velocity decay $\delta v$ and diffusion velocity $\langle \Delta v_1 \rangle$ at the mesolevel-1 lie closely corresponds to the criterion (3.2). After impact velocity ~295 m/s the free surface velocity decay increases and spall-strength of steel decreases.

**Table 6.** Results of test for the 2-nd set of 38ХН3МФА steel.

| N | Target thickn., mm | Impactor thickn., mm | Impact vel. $U_{imp}$, m/s | Decay f.s vel. δv, m/s | Diffusion velocity, $\langle \Delta v_1 \rangle$, m/s | Pull-back velocity, *W*, m/s |
|---|---|---|---|---|---|---|
| 20k | 4.27 | 2.11 | 200.3 | 21 | 0 | 159 |
| 38k | 4.85 | 1.9 | 230 | 54.1 | 0 | 139.3 |
| 28k | 4.90 | 2.05 | 242 | 55.6 | 15.6 | 166 |
| 19k | 4.25 | 2.12 | 252 | 22 | 0 | 193 |
| 18k | 4.90 | 1.97 | 261 | 19 | 0 | 175 |
| 36k | 4.95 | 2.05 | 300 | 58 | 26 | 179 |
| 33k | 5.05 | 2.00 | 308 | 27 | 23.6 | 212 |
| 22k | 4.26 | 2.15 | 308 | 0 | 42 | 237 |
| 31k | 4.88 | 2.00 | 310 | 65 | 39.3 | 176.2 |
| 30k | 5.00 | 2.05 | 334 | 67 | 36.4 | 167 |
| 35k | 4.95 | 2.00 | 338 | 85 | 29 | 153 |

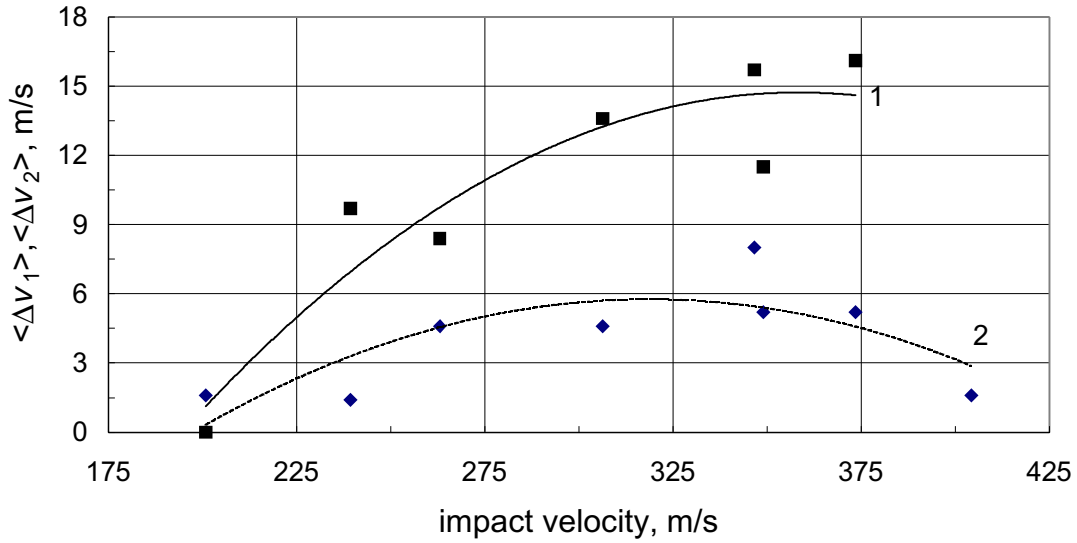


**Fig.3.13.** Diffusion velocity at the mesolevel-1 $\langle \Delta v_1 \rangle$ (1), mesolevel-2 $\langle \Delta v_2 \rangle$ (2) versus impact velocity (1-st set of 38ХН3МФА steel).

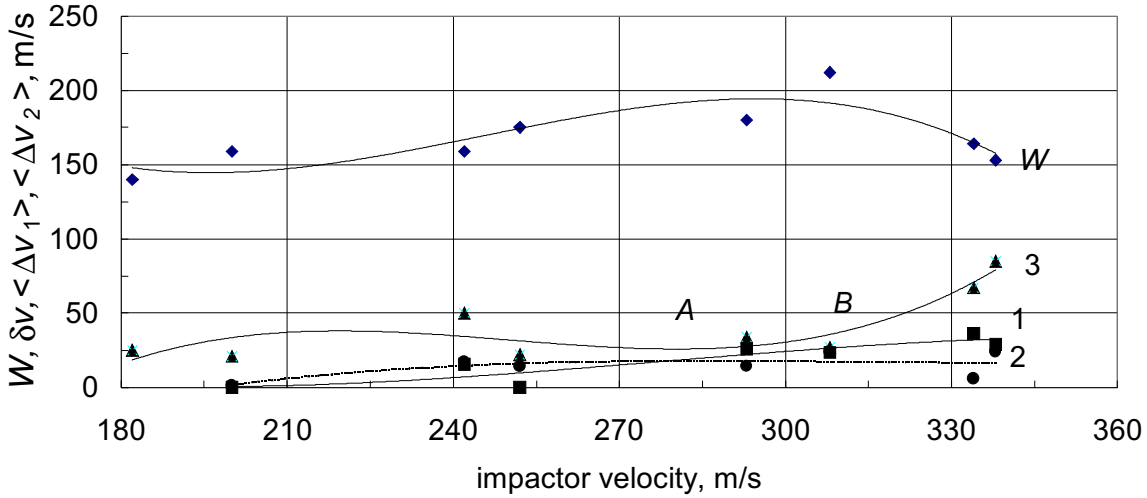


**Fig.3.14.** Diffusion velocity at the mesolevel-1 $\langle \Delta v_1 \rangle$ (1), mesolevel-2 $\langle \Delta v_2 \rangle$ (2), velocity decay $\delta v$ (3) and pull-back velocity $W$ versus impact velocity (2-nd set of 38ХН3МФА steel).

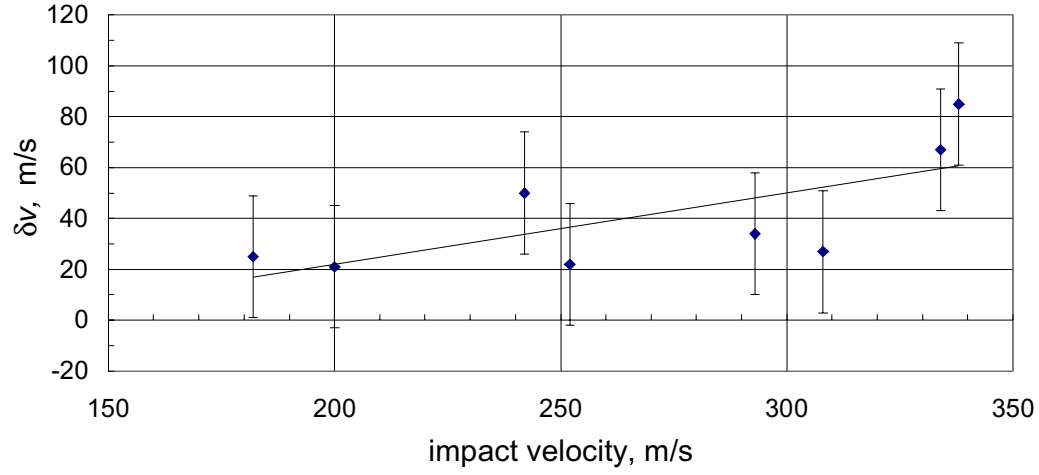


**Fig.3.15.** Velocity decay versus impact velocity (2-nd set of 38ХН3МФА steel).

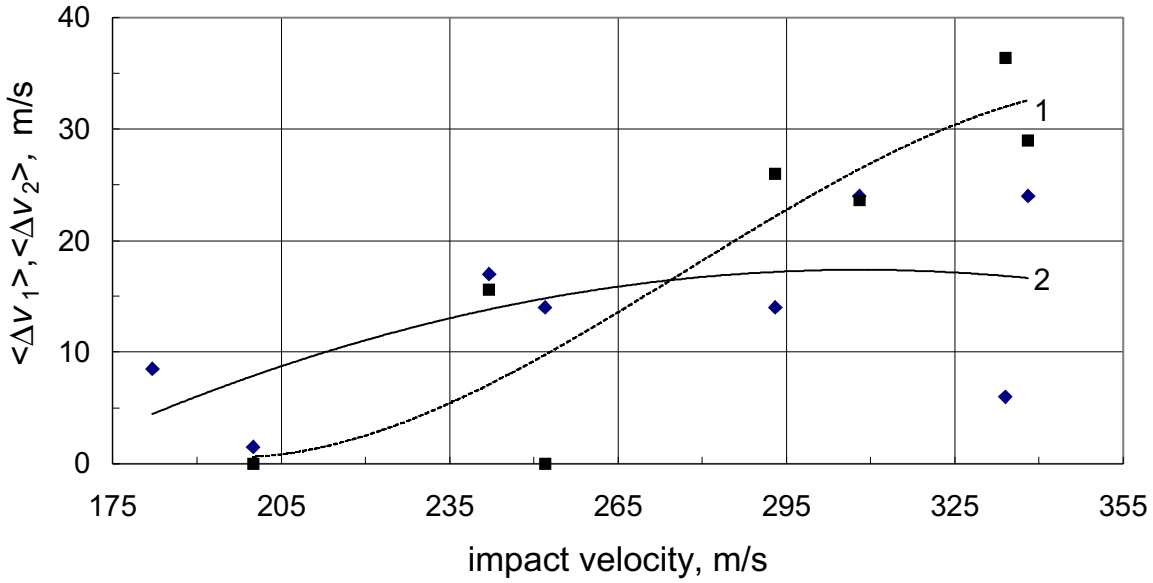


**Fig.3.16.** Diffusion velocity at the mesolevel-1 $\langle \Delta v_1 \rangle$ (1), mesolevel-2 $\langle \Delta v_2 \rangle$ (2) versus impact velocity (2-nd set of 38ХН3МФА steel).

3). 4340 steel.

This is a complex alloyed ductile steel (HRc 40). Results of tests are provided in Tables 7-8.

Dependencies of pull-back velocity, free surface velocity decay and diffusion velocity on the impact velocity are provided in Fig.3.17. Dependence of pick free surface velocity on the impact velocity is presented in Fig. 3.18. It may be seen that pick velocity draws near the impact velocity at high strain rates.

Dependencies $\langle \Delta v_1 \rangle = f(U_{imp})$ and $\delta v$ lie closely so the criterion (3.2) is satisfied. The intersection of the kinetic characteristics of structure just corresponds to the smooth maximum for the pull-back velocity. To check the criterion (3.1) in Fig. 3.19 the free surface velocity decay $\delta v = f(U_{imp})$ is presented separately. It is seen from Fig. 3.20 that criterion (3.1) is also fulfilled and all the dependencies show a monotonous behavior within the impact velocities under investigation.

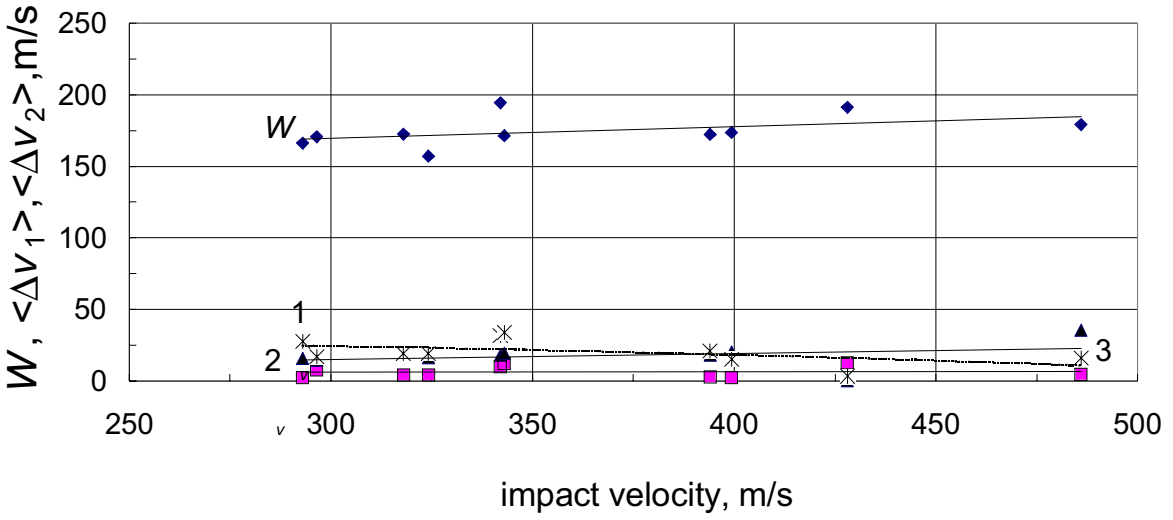


**Fig.3.17.** Diffusion velocity at the mesolevel-1 (1) $\langle \Delta v_1 \rangle$, mesolevel-2 (2) $\langle \Delta v_2 \rangle$, defect of the free surface velocity $\delta v$ (3) and pull-back velocity $W$ versus impact velocity (4340 steel).

**Table 7.** Results of test for the 4340 steel.

| N | Target thick., mm | Impactor thick., mm | Impact vel., m/s | Maximum vel., m/s | Decay of vel. $\delta v$, m/s | Diffusion velocity, $\langle \Delta v_1 \rangle$, m/s | Pull-back velocity, $W$, m/s |
|---|---|---|---|---|---|---|---|
| 1 | 4.98 | 1.86 | 293 | 265.6 | 27.4 | 15.6 | 166.2 |
| 2 | 5.00 | 1.80 | 296.5 | 279.6 | 16.9 | 14.4 | 170.6 |
| 3 | 4.94 | 1.92 | 318 | 298.6 | 19.2 | 18.0 | 172.5 |
| 4 | 4.98 | 1.88 | 324.2 | 305.2 | 19.0 | 16.1 | 157.2 |
| 5 | 4.93 | 1.52 | 342 | 310.1 | 31.9 | 18.1 | 194.5 |
| 6 | 5.00 | 1.96 | 343 | 309.3 | 33.7 | 19.4 | 171.5 |
| 7 | 4.94 | 1.88 | 394 | 373.1 | 20.9 | 18.3 | 172.3 |
| 8 | 4.94 | 1.91 | 399.3 | 384.2 | 15.1 | 20.1 | 173.7 |
| 9 | 4.94 | 2.06 | 428 | 424.8 | 3.2 | – | 191.3 |
| 10 | 4.94 | 1.88 | 486 | 472.7 | 16.2 | 35.5 | 179.3 |
| 11 | 4.94 | 1.84 | 550 | – | – | – | –*) |

*) In this case pull-back velocity and other characteristics couldn't be determined because of lost of the interference signal intensity. The character of the interference signal allows to suppose that there was a turning of grain on the free surface.

**Table 8**. Results of calculation of stress-strain diagram for the 4340 steel.

| N | Target thick., mm | Impact thick., mm | Imp. vel., m/s | Spall-stress GPa | HEL vel., m/s | Plastic vel. $C_p^1$, km/s | Stress $\sigma$, GPa | Strain $\varepsilon$ $10^{-2}$ |
|---|---|---|---|---|---|---|---|---|
| 1 | 4.98 | 1.86 | 293 | 3.1 | 100 | 4.95 | 4.34 | 2.5 |
| 2 | 5.0 | 1.8 | 296.5 | 3.37 | 100 | 4.97 | 5.86 | 3.05 |
| 3 | 4.94 | 1.92 | 318 | 3.45 | 95.4 | 5.0 | 6.24 | 2.83 |
| 4 | 4.98 | 1.88 | 324.2 | 3.1 | 95.0 | 4.98 | 6.35 | 2.9 |
| 5 | 4.93 | 1.52 | 342 | 4.03 | 100 | 5.02 | 6.5 | 2.93 |
| 7 | 5.00 | 1.96 | 343 | 3.14 | 71.88 | 4.84 | 6.2 | 3.05 |
| 8 | 4.94 | 1.88 | 394 | 3.49 | 100 | 5.02 | 7.74 | 3.55 |
| 9 | 4.94 | 1.91 | 399.3 | 3.56 | 105.8 | 5.02 | 7.98 | 3.63 |
| 10 | 4.93 | 2.06 | 428 | 3.92 | 100 | 4.97 | 8.69 | 4.1 |
| 11 | 4.86 | 1.88 | 4.86 | 3.6 | 100 | 4.88 | 9.53 | 4.82 |

Stress-strain diagram for the 4340 steel is provided in Fig. 3.21.

4). 16X11H2B2MΦ steel.

This is a complex alloyed ductile steel of moderate hardness (HRc 37). This kind of steel having an increased content of Cr, W, Mo, V, Nb and B is used for details of gas turbines steam-power plants. Being sufficient strength, the steel belongs to the so-called heat-resistance materials. From the point of view of mechanical behavior this steel is characterized by more high plasticity compared the previous kinds steel though its dynamic strength remains sufficiently high. Results of tests and calculation of stress-strain diagram for 16X11H2B2MΦ steel are provided in Tables 9 and 10.

Dependencies of pull-back velocity $W$ and diffusion velocities $\langle \Delta v_1 \rangle$ at the mesolevel-1 and $\langle \Delta v_2 \rangle$ at the mesolevel-2 on the impact velocity are presented in Fig. 3.22. In this figure we also present a value of the free surface velocity decay at the mesolevel-2 $\delta v$. One can see that the criterion (3.1), i.e. condition where diffusion velocity at the mesolevel-1 becomes higher than the diffusion velocity at the mesolevel-2 (i.e. $\langle \Delta v_1 \rangle > \langle \Delta v_2 \rangle$) is sat-

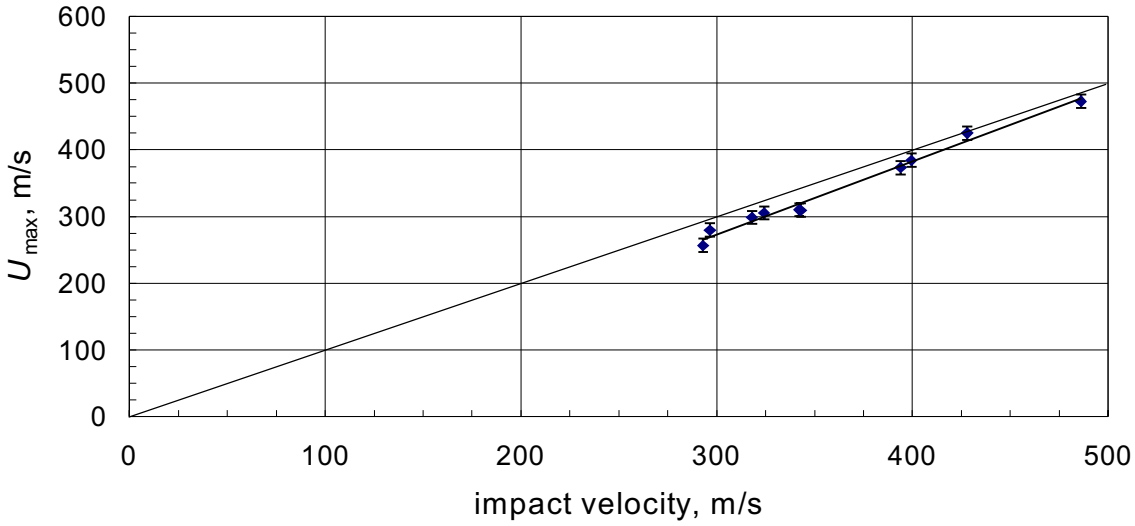


**Fig.3.18.** Dependence of the maximum free surface velocity on the impact velocity (4340 steel).

isfied within overall range of impact velocities. (point A in Fig. 3.22). This means that the velocity scattering at the mesolevel-2 cannot be seen on the background of the velocity scattering at the mesolevel-1. In this case all the processes of dynamic fracture within the spall zone are determined by the kinetics of structure at the mesolevel-1. Just the kinetics of microstructure at the mesolevel-1 characterizes an effectiveness of relaxation of internal stresses during the dynamic fracture. In our case stress relaxation processes at the mesolevel-1 suppress a development of shear banding resulting from the velocity scattering at the mesolevel-2. As a result, the spall-strength of material is invariable within the impact velocities under investigation. In Fig. 3.23 a free surface velocity $U_{max}$ as a function of the impact velocity is provided separately. In this figure we also present a curve corresponding to the impact velocity. One can see that free surface velocity at the plateau of compressive pulse smaller than impact velocity for every shot approximately by 15-20 m/s although there is a scattering of this deviation from

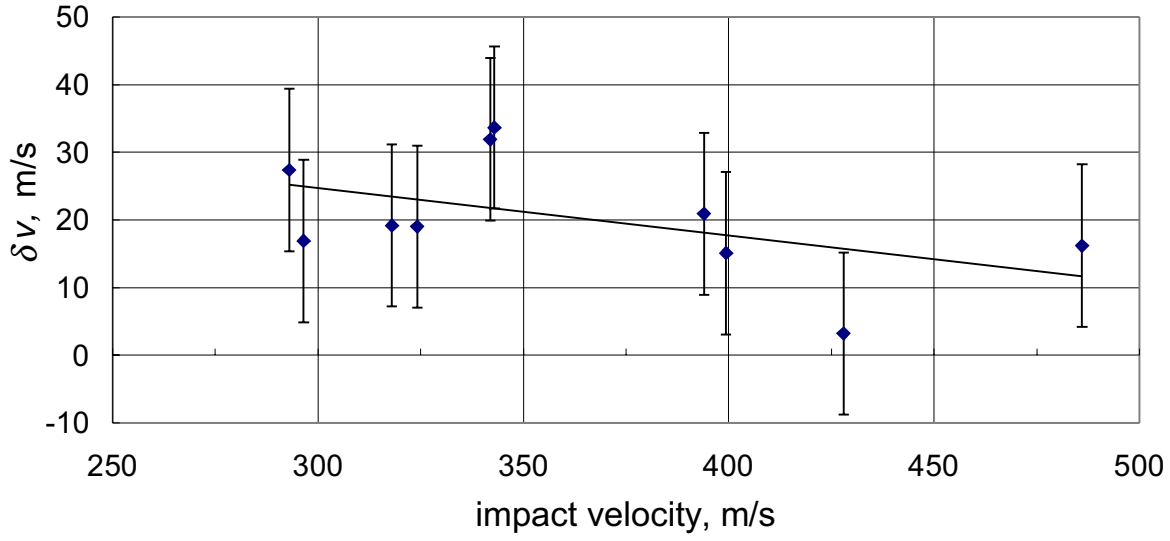


**Fig.3.19.** Velocity decay versus impact velocity (4340 steel).

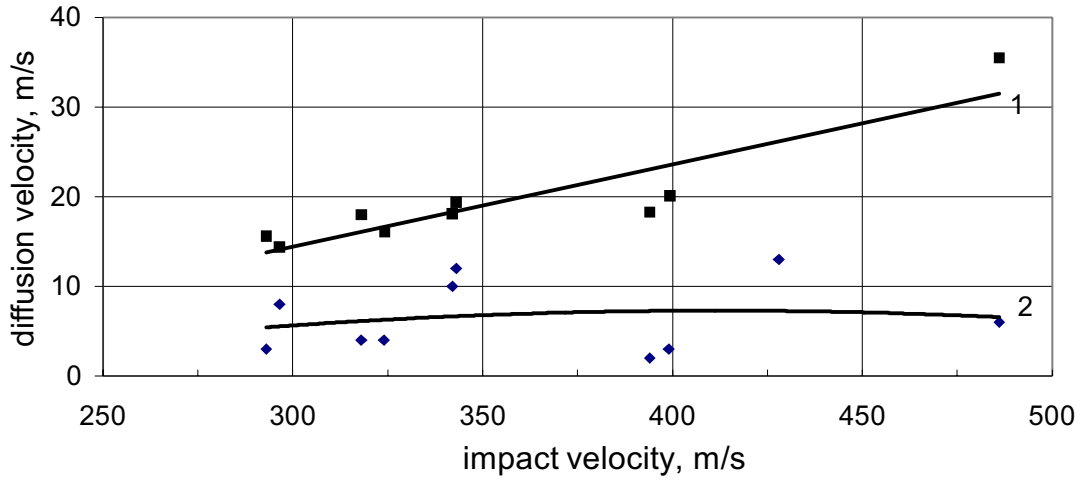


**Fig.3.20.** Diffusion velocity at the mesolevel-1 $\langle \Delta v_1 \rangle$ (1), mesolevel-2 $\langle \Delta v_2 \rangle$ (2) versus impact velocity (4340 steel).

one shot to another. In Fig. 3.24 a dependence of free surface velocity decay on the impact velocity is presented together with deviations of velocity. In Fig. 3.22 this curve crosses the diffusion velocity $\langle \Delta v_1 \rangle$ at the impact velocity of 310 m/s. This means that criterion (3.2) is also fulfilled. Thus, 16X11H2B2MΦ steel is the example of optimized material where both criteria of high plasticity and high strength are passed.

Normal stress and strain at the plastic front are calculated by using the formulae (2.1-2.2). Stress-strain diagram for the 16X11H2B2MΦ steel is provided in Fig. 3.25.

5). 28X3HCMBΦA steel.

The fifth kind of steel tested in the frame of present study is a complex alloyed 28X3HCMBΦA steel. This steel is ordinary used in annealed state to provide a high plasticity (HRc 25). Results of tests are presented in Table 11. Dependencies of pull-back velocity $W=f(U_{imp})$, diffusion velocity $\langle \Delta v_1 \rangle = f(U_{imp})$ and defect of the free surface velocity $\delta v = f(U_{imp})$ on the impact velocity are provided in Fig. 3.26. The

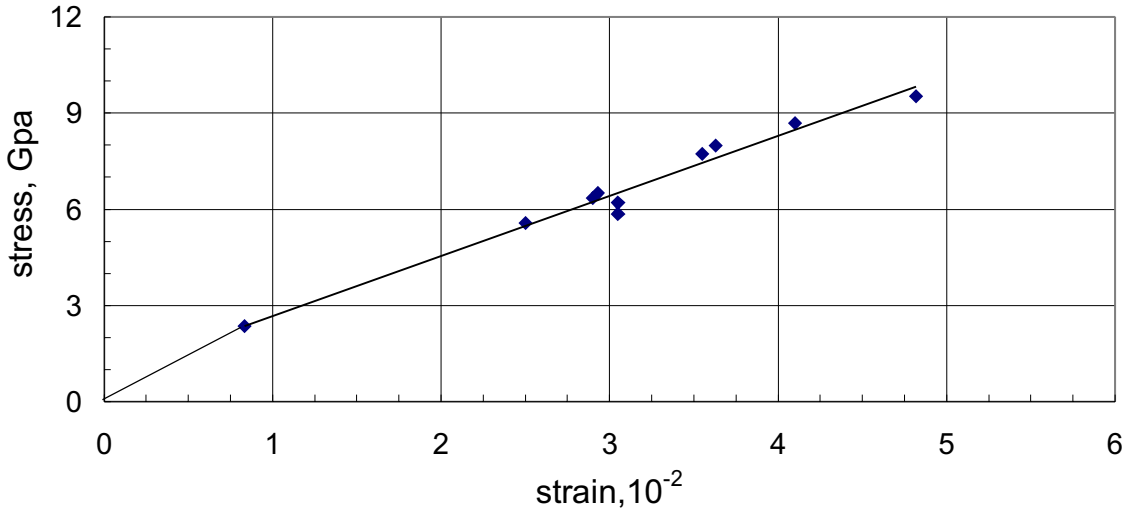


**Fig.3.21.** Stress-strain diagram for the 4340 steel.

**Table 9.** Results of test for 16X11H2B2MΦ steel.

| N | Target thick., mm | Impactor thick., mm | Impact. vel., m/s | Max.f. s. vel. $U_{max}$, m/s | Decay of vel. $\delta v$, m/s | Meso-1 dispers. $\Delta V_1$, m/s | Pull-back velocity, $W$, m/s |
|---|---|---|---|---|---|---|---|
| 1 | 4.76 | 2.05 | 172.4 | 154.2 | 0 | – | – |
| 2 | 4.76 | 2.03 | 233.5 | 225.6 | 7.3 | 9.80 | 161.4 |
| 3 | 4.76 | 2.03 | 255.0 | 240.1 | 0.7 | 11.21 | 159.0 |
| 4 | 4.75 | 2.05 | 291.5 | 273.4 | 1.3 | 17.1 | 154.4 |
| 5 | 4.76 | 2.05 | 305.5 | 290.5 | 3.3 | 14.4 | 165.0 |
| 6 | 4.75 | 2.04 | 366.5 | 360.7 | 0 | 19.0 | 160.2 |
| 7 | 4.76 | 2.03 | 378.3 | 359.8 | 6.3 | 22.9 | 163.8 |
| 8 | 4.75 | 2.05 | 413.0 | 374 | 3.3 | 29.9 | 120.6 |
| 9 | 4.74 | 2.03 | 421.0 | 402.6 | 0.3 | 29.8 | 163.2 |

**Table 10.** Results of calculations of stress-strain diagram for 16X11H2B2MΦ steel.

| N | Target thick., mm | Impact thick., mm | Imp. vel., m/s | Delay $\Delta t_1$, ns | HEL vel., m/s | Plastic vel. $C_p^1$, km/s | Stress σ, GPa | Strain $\varepsilon\ 10^{-2}$ |
|---|---|---|---|---|---|---|---|---|
| 1 | 4.74 | 2.03 | 421 | 155 | 44 | 4.98 | 7.99 | 3.97 |
| 2 | 4.75 | 2.05 | 413 | 153 | 51 | 4.99 | 7.47 | 3.67 |
| 3 | 4.75 | 2.04 | 366.5 | 150 | 50.0 | 5.01 | 7.23 | 3.52 |
| 4 | 4.76 | 2.03 | 378.3 | 155 | 46.0 | 4.98 | 7.16 | 3.54 |
| 5 | 4.76 | 2.05 | 305 | 150 | 52 | 5.01 | 5.87 | 2.82 |
| 6 | 4.75 | 2.05 | 291.5 | 170 | 48 | 4.91 | 5.43 | 2.7 |
| 7 | 4.76 | 2.03 | 255 | 155 | 40 | 4.98 | 4.81 | 2.35 |
| 8 | 4.76 | 2.03 | 233 | 150 | 52 | 5.01 | 4.60 | 2.17 |
| 9 | 4.76 | 2.05 | 172.4 | 125 | 44 | 5.14 | 3.23 | 1.44 |

first what one can see that the velocity decay for that material lies more higher than the diffusion velocity. This means that the local stresses don't relax, which creates the favorable conditions for activation of meselevel-2 responsible for dynamic fracture of material.

It seems to be interesting to find the impact velocity where dispersions at the mesolevel-1 and mesolevel-2 become comparable each other. To determine the average value of the diffusion velocity at the mesolevel-2, in Fig. 3.27 the dependence velocity decay is presented together with random deviations of this within impact velocity range. In Fig. 3.28 the deviation versus impact velocity is plotted separately. This curve has the obvious maximum at the impact velocity of 210 - 230 m/s. In this figure we also present the diffusion velocity for the mesolevel-1 determined directly from the interferometric measurements. Intersection of these curves happens under impact velocity of 235 m/s. This point corresponds the impact velocity where diffusion velocity at the mesolevel-1 becomes higher than that at the mesolevel-2. Pull-back velocity also begins to increase. However, since the defect of the average velocity $\delta v$ remains to be more higher than the diffusion velocity at the mesolevel-1 $\langle \Delta v_1 \rangle$ the effect of the velocity distribution at the mesolevel-1 may be insignificant (criterion (3.2) isn't fulfilled).

## 4. MICROSTRUCRUE INVESTIGATIONS

**1). 40XCHMA steel.** Standard regime of thermal treatment supposes a low tempering, so that structure of steel consists of martensite plus low beinit.

According to interferometric measurements, for that kind of steel the following combination kinetic criteria works practically within overall range of impact velocities:

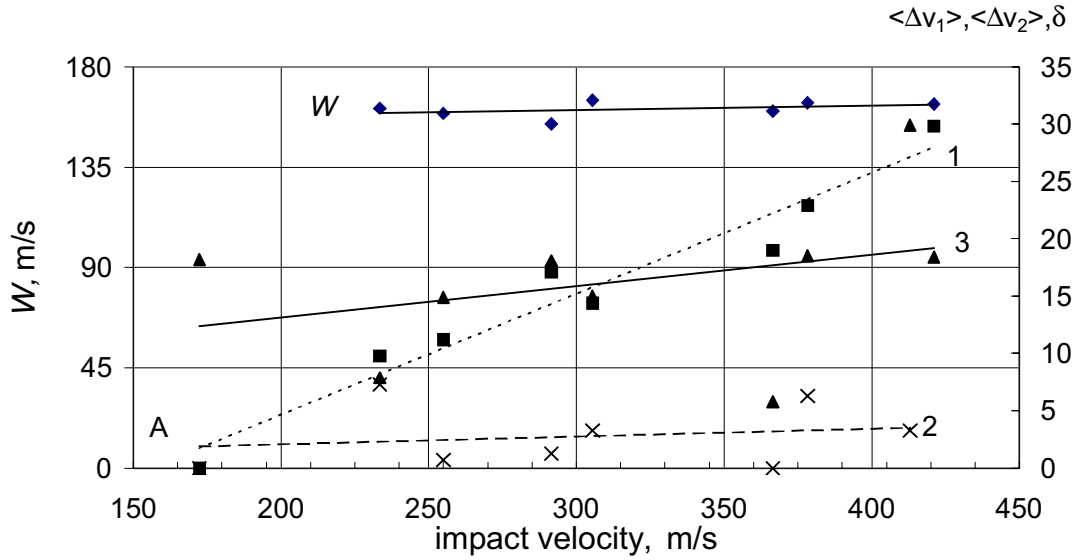


**Fig.3.22.** Dependencies of pull-back velocity *W,* diffusion velocity at the mesolevel-1 $\langle \Delta v_1 \rangle$ (1), mesolevel-2 $\langle \Delta v_2 \rangle$ (2) and velocity decay $\delta v$ (3) on the impact velocity (16X11H2B2MΦ steel).

a) $\langle \Delta v_1 \rangle > \langle \Delta v_2 \rangle$,
b) $\langle \Delta v_1 \rangle < \delta v$. (4.1)

Typical pattern of spallation at the lower boundary of the impact velocities in the form of cleavage, which seems to be the most proper mechanism of fracture for that kind of steel, is presented in Fig. 4.1. There is a lot of plane cracks parallel to the free surface of target, the length of which ranges from 1.5 mm to 10 mm. As a rule, the spall crack looks a continuous crack parallel to the free surface of target having a small longitudinal steps Using the marking accepted in Fig. 1.1 it may be said that spall crack in the 40XCHMA steel consists of pieces of *D* and *h* sizes. The character of spall fracture conserved over the impact velocities under investigation although at the upper range of impact velocities, together with *h*-pieces, *H*-pieces also appear. The latter are the adiabatic shears band of 400μm length linking the *D*-pieces of identical size.

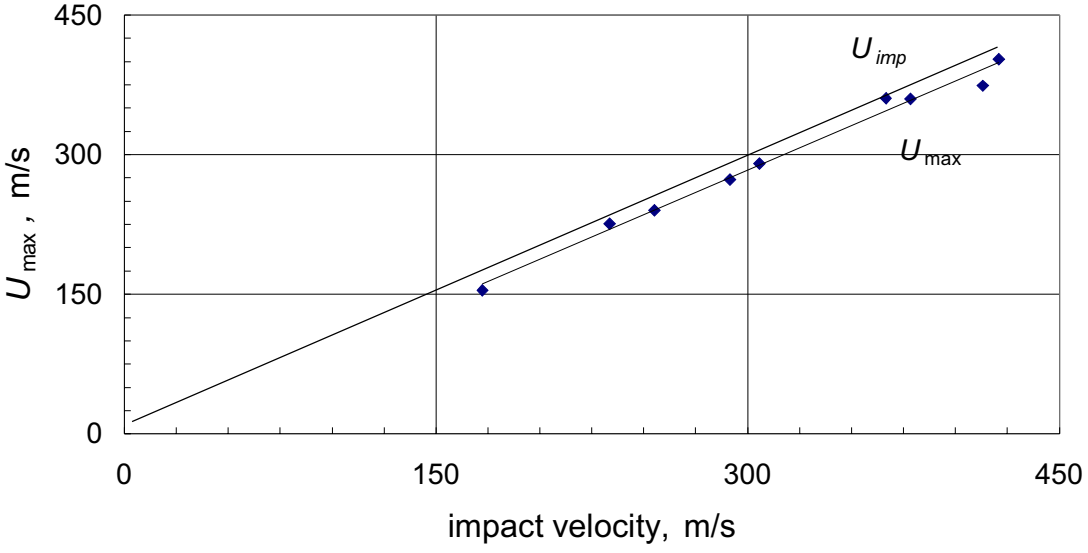


**Fig.3.23.** Maximum free surface velocity versus impact velocity (16X11H2B2MΦ steel).

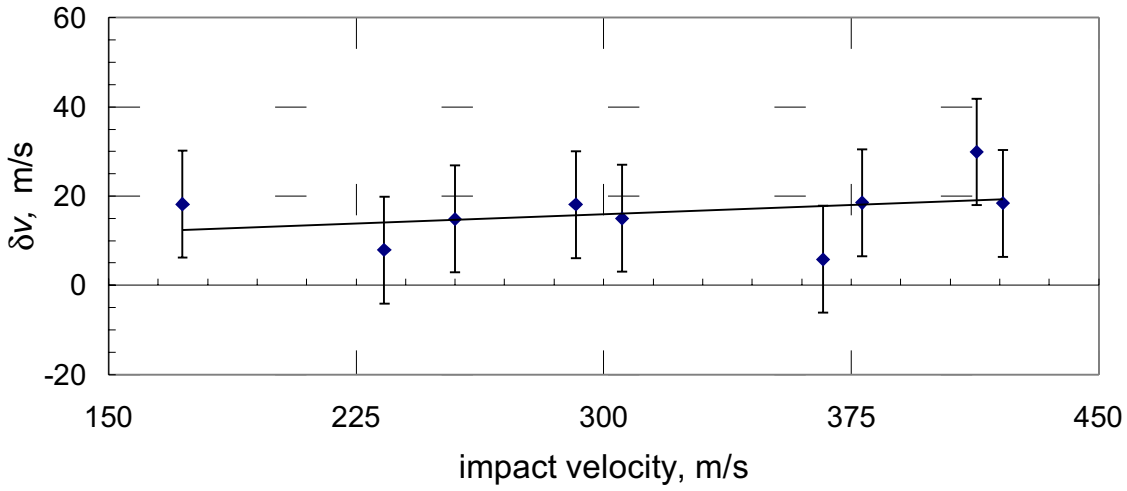


**Fig.3.24.** Dependence the free surface velocity decay $\delta v$ on the impact velocity (16X11H2B2MΦ steel).

Typical example of similar fracture is presented in Fig. 4.2.

Dynamic fracture of the second set of 40XCHMA steel targets has a slightly differ character.

Kinematical mechanism of spall fracture turns out to be different at different regions of impact velocity range. At the low boundary of that range there is a following combination of the kinetic characteristics of mesostructure:

a) $\langle \Delta v_1 \rangle > \langle \Delta v_2 \rangle$,

b) $\langle \Delta v_1 \rangle < \delta v$.

The spall crack has a step-like shape with identical longitudinal and transverse length of steps dimensions of which belong to mesolevel-2 (100-150μm).

At the impact velocity of 499 m/s where the spall-strength is maximum the following conditions are fulfilled:

a) $\langle \Delta v_1 \rangle = \langle \Delta v_2 \rangle$,

b) $\langle \Delta v_1 \rangle = \delta v$. (4.2)

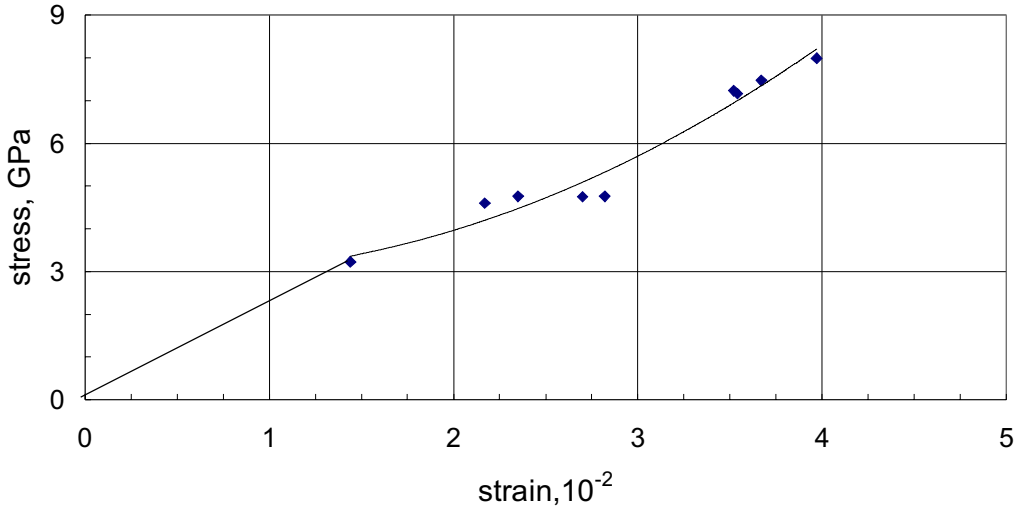


**Fig.3.25.** Stress-strain diagram for the (16X11H2B2MΦ steel).

**Table 11**. Results of tests for the 28X3HCMBΦA steel.

| N | Target thick., mm | Impactor thick., mm | Impact. vel., m/s | Max.f. s. vel. $U_{max}$, m/s | Decay of vel. $\delta v$, m/s | Meso-1 dispers. $\Delta V_1$, m/s | Pull-back velocity, $W$, m/s | HEL, m/s |
|---|---|---|---|---|---|---|---|---|
| 10a | 9.97 | 3.1 | 97.5 | * | * | * | 52 | 25 |
| 21a | 9.96 | 3.07 | 130.9 | 83.3 | 47.6 | 0 | 73.6 | 43 |
| 18a | 10.58 | 3.1 | 142.2 | 90 | 52.2 | 0 | 52 | 40 |
| 17a | 10.42 | 3.09 | 152.5 | 116 | 36.6 | 0 | 79 | 50 |
| 15a | 9.27 | 3.09 | 155.5 | 126 | 55.5 | 0 | 73.8 | 47 |
| 16a | 10 | 3.09 | 180.5 | 116 | 68 | 9.8 | 67.8 | 35 |
| 6a | 10 | 3.1 | 195.1 | 152 | 23 | 11.96 | * | 60.7 |
| 12a | 8.97 | 3.09 | 196 | 164 | 52.7 | 12.4 | 68.6 | 55 |
| 8a | 9.96 | 3.09 | 196.3 | 165 | 29 | 12.3 | 75 | 50 |
| 29a | 11.87 | 2.92 | 213 | 182 | 77.4 | 12.5 | 87 | 50 |
| 5a | 9.99 | 3.09 | 269 | 190 | 59 | 23 | 69 | 50 |
| 2a | 10.1 | 3.09 | 308 | 256 | 51.5 | 13 | 66.3 | 57 |
| 4a | 10.0 | 3.07 | 311 | 265 | 44 | 24.3 | 75 | 50 |
| 3a | 10.01 | 3.1 | 318 | 270 | 48.3 | 12.3 | 77.5 | 50 |
| 25a | 8.54 | 3.05 | 350 | 307 | 43 | 24 | 87 | 39 |
| 23a | 8.46 | 3.08 | 376 | 350 | 26 | 18.3 | 97 | 60 |
| 31a | 11.7 | 2.87 | 380 | 326 | 54 | 35 | 126 | 60 |

and within the spall zone there is a dense network of short adiabatic shear bands (Fig. 4.3). In case of ductile steel a rotational cell structure would be nucleated under condition (4.2). For the brittle steel such as 40XCHMA steel, instead of rotational kinematical mechanism of deformation and fracture, another three-dimensional structure is realized, namely dense network of short adiabatic shear bands, also provided a maximum spall strength of material.

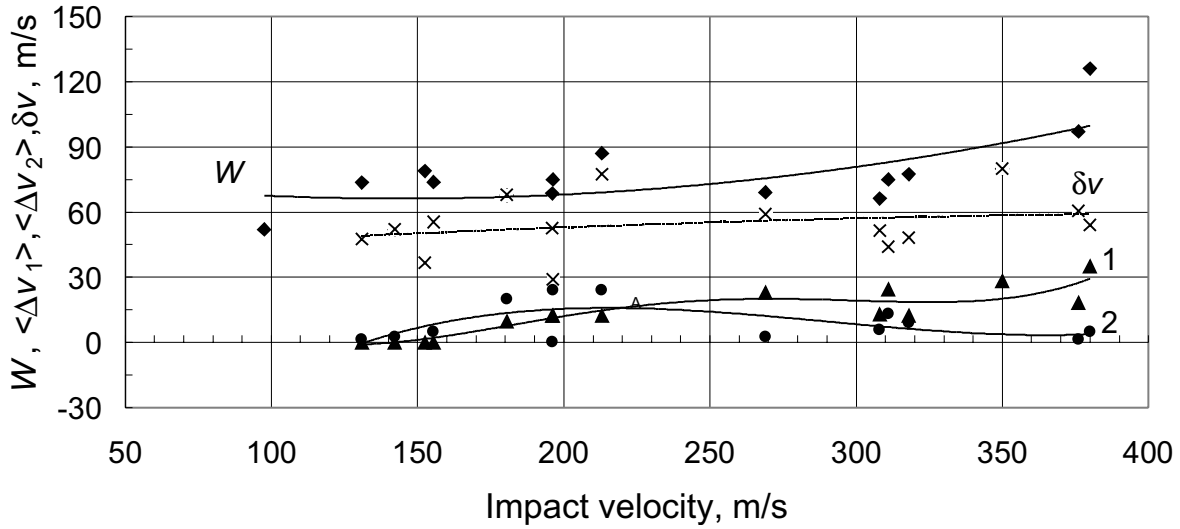


**Fig.3.26.** Pull-back velocity $W$, diffusion velocity at the mesolevel-1 $\langle \Delta v_1 \rangle$ (1), mesolevel-2 $\langle \Delta v_2 \rangle$ (2), and defect of the free surface velocity $\delta v$ versus impact velocity (28X3CHMBΦA steel).

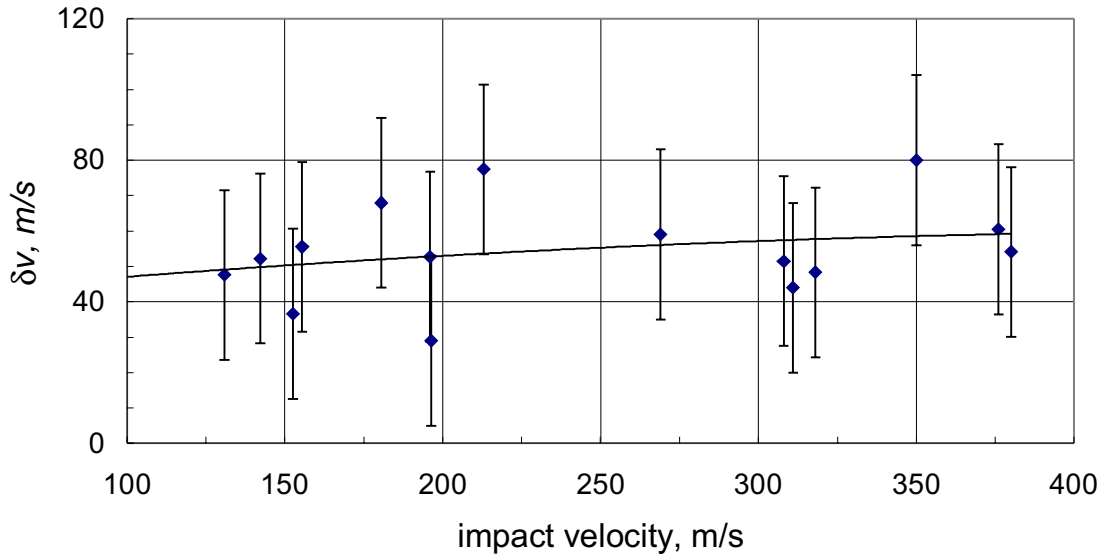


**Fig.3.27.** Defect of the free surface velocity versus impact velocity (28X3CHMBΦA steel).

At the impact velocity of 521 m/s as shown in Fig.3.6 criterion (3.1) is fulfilled. In this situation nucleation of crack is controlled by the diffusion velocity at the mesolevel-1 and kinetic characteristics are satisfy to the following conditions:

$$\text{a) } \langle \Delta v_1 \rangle > \langle \Delta v_2 \rangle, \qquad \text{b) } \langle \Delta v_1 \rangle < \delta v. \tag{4.3}$$

In this case the dimensions of crack are more smaller than those under condition of $\langle \Delta v_1 \rangle << \langle \Delta v_2 \rangle$ when the length of horizon pieces of cracks (*D*-pieces) equals $2C_0 t_{sp} = 500$ mm. Here $C_0$ is the volume sound velocity and (for steel $C_0$ = 4.71 km/s) and $t_{sp}$ = 100 ns is the duration of spall fracture process (the so-called horizon scale introduced by Grady [16]).

At the same time, for the impact velocity of 521 m/s the condition (3.2) isn't fulfilled. In this case an

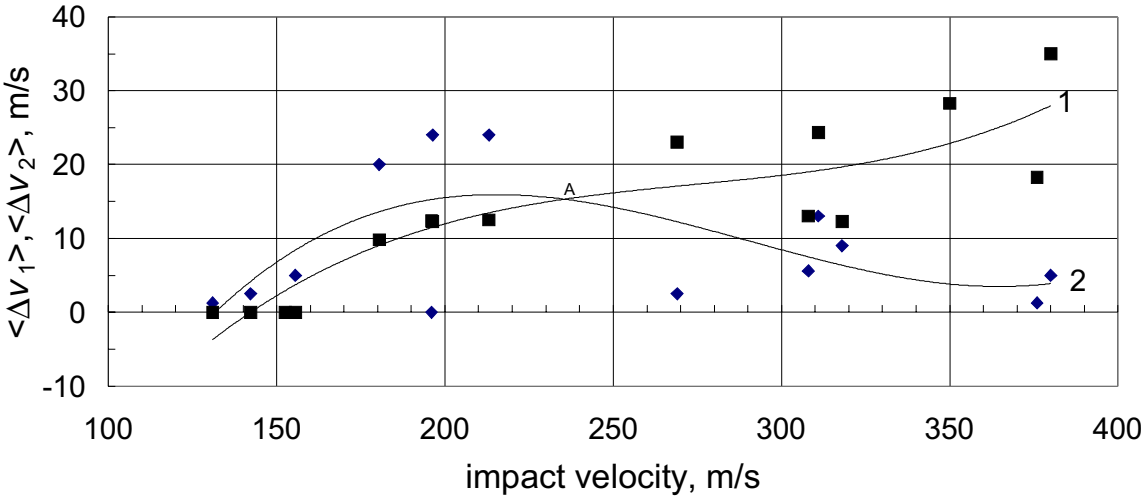


**Fig.3.28.** Diffusion velocity at the mesolevel-1 $\langle \Delta v_1 \rangle$ (1), mesolevel-2 $\langle \Delta v_2 \rangle$ (2) versus impact velocity (28X3CHMBΦA steel).

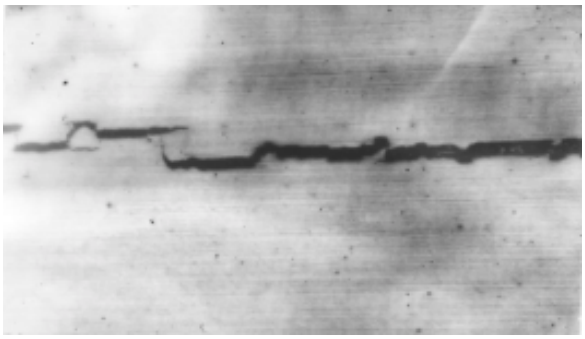

**Fig.4.1.** Large-scale (*D* and *H*) cleavage kind of spallation in 40XCHMA steel target (1-st set) at the impact velocity of 211 m/s (magnification $32^{+}$).

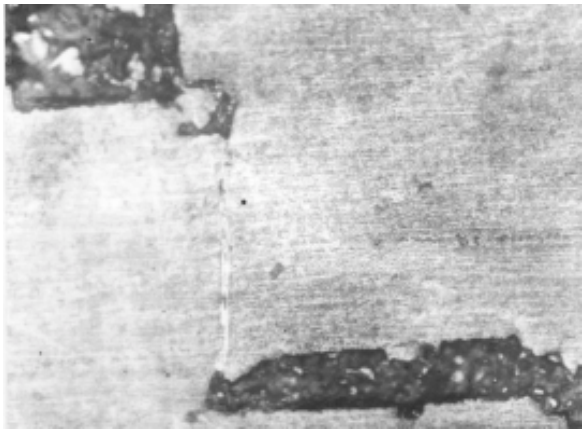

**Fig.4.2.** Adiabatic shear band in 40XCHMA steel at the impact velocity of 343 m/s (magn. $125^{+}$).

intensive pumping over the energy from mesolevel-1 to mesolevel-2 takes place. It will be shown in Section 5, that the spall strength must decrease, which is seen in Fig.3.6, while cleavage again becomes the basic kinematic mechanism of failure (see Fig.4.4).

2). 38XH3MΦA steel.

The first cracks in the post-shocked specimens are found at the impact velocity of 181,3 m/s. A spall-gap is practically formed at the impact velocity of 221,2 m/s. Kinetic criteria (3.1) is fulfilled within overall range of impact velocities, which means that mesolevel-2 isn't activated. This explains why the large-scale longitudinal cracks within the spall zone are absent. In Fig. 4.5 one can see only small-scale longitudinal and transverse cracks. As for the criterion (3.2). It isn't fulfilled up to impact velocity of 350 m/s. That is why a basic mechanism of dynamic fracture here is the cleavage. Thus, lower the impact velocity of 350 m/s there is a following

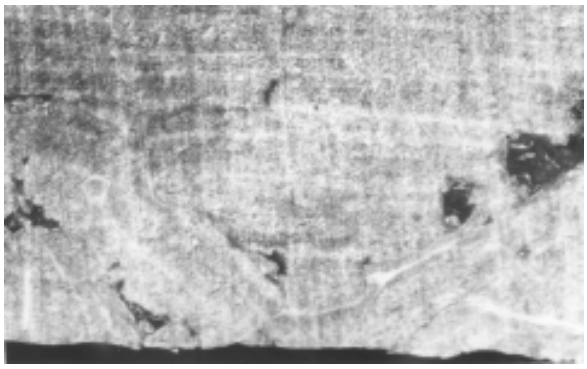

**Fig.4.3.** Dense network of adiabatic shear bands within the spall zone of 40XCHMA steel target at the impact velocity of 499 m/s (magnification $200^{+}$).

relationship between diffusion velocities at the mesoscopic sublevels:

a) $\langle \Delta v_1 \rangle > \langle \Delta v_2 \rangle$,

b) $\langle \Delta v_1 \rangle < \delta v$.

After impact velocity of 350 m/s, as it's seen from Fig 3.9 in the 38XH3MΦA steel a following combination of kinetic characteristics begins to work:

a) $\langle \Delta v_1 \rangle > \langle \Delta v_2 \rangle$,

b) $\langle \Delta v_1 \rangle > \delta v$.

So one may expect a change of kinematical mechanism of fracture at the mesolevel. Indeed, micro structure study show that instead of cleavage after impact velocity of 350 m/s a viscous fracture in the form of nucleation and grow of pores is realized (see Fig. 4.6).

3). 4340 steel.

This is a complex alloyed ductile steel with a structure of sorbit oriented along martesite (HRc 40). Interference response shows spallation at the impact velocity of 293 m/s. The seats of damage look like separate cracks parallel to the free surface of target. There are no longitudinal shear bands linking the transverse cracks. At the same time, under impact velocity of 296.4 m/s the of longitudinal shear bands appear, so the impact velocity of 296.4 m/s can be considered as threshold impact velocity providing a critical strain rate at which shear bands are irreversibly nucleated within the spall zone. One can estimate a length of shear band corresponding critical strain rate as follows:

$$L_{cr} = \langle \Delta v_2 \rangle t_{sp.}, \qquad (4.4)$$

**Fig.4.4.** Large-scale (*D* and *H*) cleavage kind of spallation in 40XCHMA steel target (1-st set) at the impact velocity of 521 m/s (magnification 200+).

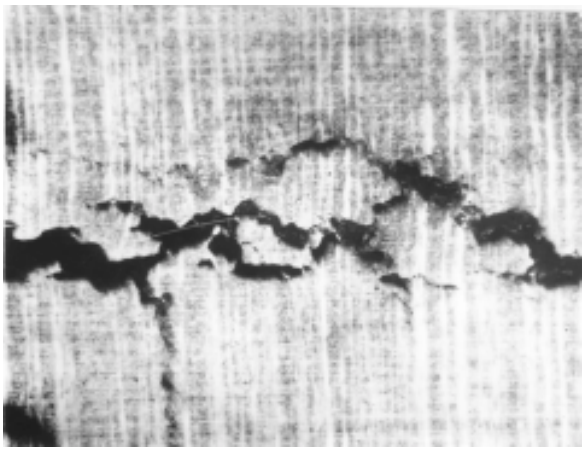

**Fig.4.5.** Small-scale (*d* and *h*) cleavage spallation in 38XH3MΦA steel at the impact velocity of 221 m/s (magn. 32+).

**Fig.4.6.** Evolution of spallation mechanism in 38XH3MΦA steel with increasing impact velocity to 390 m/s (magn. 125+).

where $\langle \Delta v_2 \rangle$ is the diffusion velocity at the meso-level-2 and $t_{sp}$ is the duration of the spallation process which is determined by the time between pulse plateau and onset of macro-spallation at the rear front of compressive pulse. ($t_{sp}$ =380 ns for $U_{imp}$ = 296.4 m/s). $\langle \Delta v_2 \rangle$ can be determined from the scattering of the free surface velocity at the plateau $U_{max}$ provided in Table 7. In Fig. 3.18 dependence $U_{max}=f(U_{imp})$ together with interval of scattering of the free surface velocity is presented. Standard velocity deviation for this curve equals 3% for the $U_{imp}$= 296.4 m/s, or $\langle \Delta v_2 \rangle$ = 8.79 m/s. Then the critical shear band length $L_{cr}$ =3.44 μm.

From the presented in Fig.3.17 dependencies $\langle \Delta v_1 \rangle = f(U_{imp})$, $\langle \Delta v_2 \rangle = f(U_{imp})$ and $\delta v = f(U_{imp})$ it follows that before the impact velocity of 370 m/s the basic mechanism of spall fracture is cleavage with identical longitudinal and transverse pieces of spall crack ($D \cong H$) (see Fig. 4.7). The vertical pieces are often the adiabatic shear bands of complex configuration (see Fig. 4.8), within the spall plate there are numerous rotational cells testifying a ductile character of spall fracture (Fig.4.9). Outside the spall zone one can see also the traces of viscous flow typical example of which is provided in Fig.4.10.

4). 16X11H2B2MΦ steel.

Both kinetic criteria ((3.1) and (3.2)) are fulfilled over all range of impact velocities under investigation:

$$\text{a) } \langle \Delta v_1 \rangle > \langle \Delta v_2 \rangle, \qquad \text{b) } \langle \Delta v_1 \rangle > \delta v. \tag{4.5}$$

so the pull-back velocity dependence lies in parallel impact velocity axis. However, the steel has an obvious character of damage along the grain boundaries (grain size ≈ 60 μm). The intergranular mechanism of spall fracture conserves within overall range of impact velocities (see Fig. 4.11.).

5). 28X3HCMBΦA steel.

According to data of Section 3 this steel is optimized in criterion (3.1) and isn't optimized in criterion (3.2). This means that between kinetic characteristics of mesostructure there is the following relationships:

$$\text{a) } \langle \Delta v_1 \rangle \cong \langle \Delta v_2 \rangle, \qquad \text{b) } \langle \Delta v_1 \rangle < \delta v.$$

**Fig.4.7.** Small-scale (*d* and *h*) cleavage mechanism of spallation in 43340 steel at the impact velocity of 318 m/s (magn. $32^{+}$).

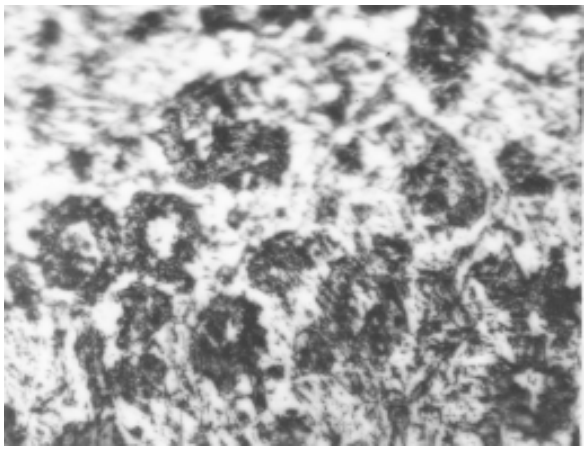

**Fig.4.9.** Rotational cells in the spall plate of 4340 steel target at the impact velocity of 343 m/s (magn. $1000^{+}$).

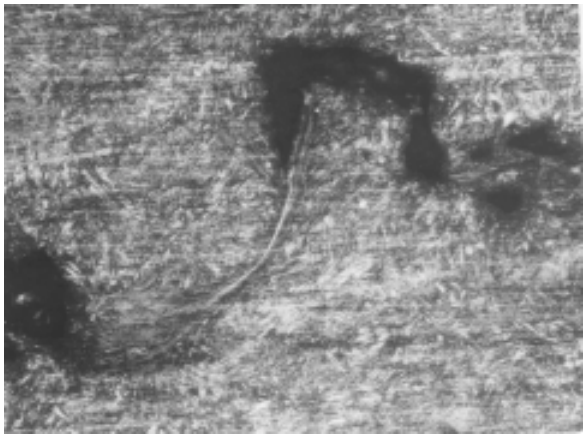

**Fig.4.8.** Adiabatic shear band linking transverse cracks in 4340 steel at the impact velocity of 318 m/s (magn. $320^{+}$).

Accordingly, the cleavage mechanism of spall fracture dominates within overall range of impact velocities. Typical picture of spall fracture for that steel is shown in Fig. 4.12.

One can see the plane cracks parallel to the free surface of target. Development of spall damage under the cleavage mechanism can be seen from Fig. 4.13. In this figure we present a dependence of summary length of all the transverse cracks in the spall plane versus impact velocity. One can see that summary length increases slowly from the impact velocity 80 m/s through 140 m/s after what the rate of cracking increases and cracking continues up to complete separation of spall plate.

## 5. ANALYSIS OF SPALL BEHAVIOR

Experimental data on spallation show that spall strength of material sensitively depends on the relation between diffusion velocity at the mesolevel-1 $\langle \Delta v_1 \rangle$ and mesolevel-2 $\langle \Delta v_2 \rangle$, on one side, (Eq. (3.1)) and between diffusion velocity $\langle \Delta v_1 \rangle$ and velocity decay $\delta v$, on another side, (Eq. (3.2)). The first criterion arises from the different roles which play diffusion velocities at the mesolevel-1 and mesolevel-2. It has previously been underlined that criterion (3.1) defines a condition when relaxation of local stresses is provided. A role of the second criterion in dynamic fracture of material is not so evident. In this connection we try to derive a dependence of spall strength on the value of the velocity decay $\delta v$. We issue from the power balance in the spall zone:

$$\frac{1}{2}\rho C v^2 = \frac{1}{2}\mu v \frac{v}{h} - \frac{1}{2}\rho C v(\delta v). \qquad (5.1)$$

Here left hand item $\frac{1}{2}\rho C v^2$ is the power which shock wave brings into spall zone, $C$ is the shock wave velocity. Item $\frac{1}{2}\mu \frac{v^2}{h}$ is the power which spends on the work of viscous forces for widening the spall gap, $\varepsilon = \frac{v}{h}$ is the strain rate related to the motion of the spall gap surfaces in opposite directions, $\mu$ is the viscosity of material and $h$ is the width of spall gap. Item $\frac{1}{2}\rho C v^2(\delta v)$ characterizes a decrease of

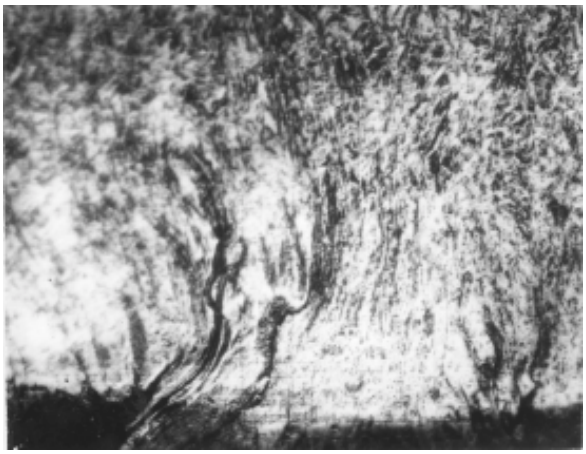

**Fig.4.10.** Viscoul flow of material within spall zone in 4340 steel at the impact velocity of 550 m/s (magn. 320+).

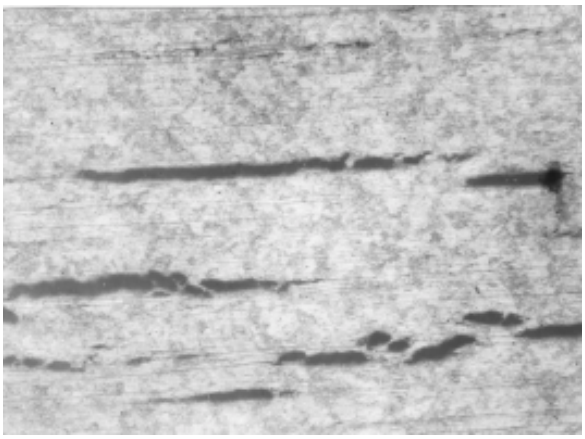

**Fig.4.12.** Large-scale (*D* and *H*) cleavage kind of spallation in 28X3CHMBΦA steel at the impact velocity of 155 m/s (magn. 32+).

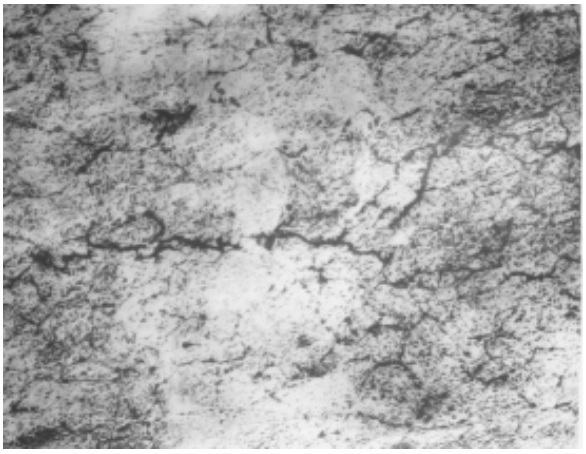

a)

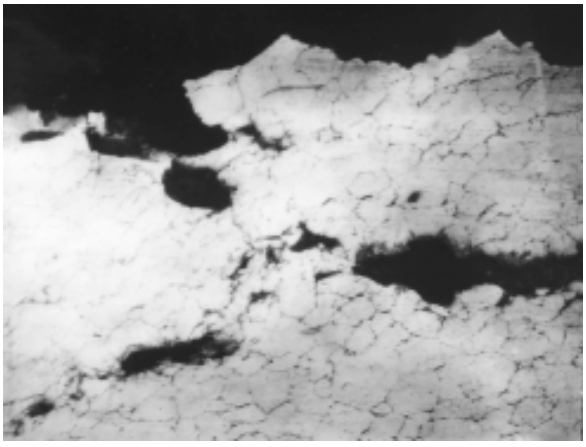

b)

**Fig.4.11.** Evolution of intergranular fracture within spall zone in 16X11H2B2MΦ steel a) impact velocity 172 m/s (magn. 200+), b) impact velocity 305.5 m/s (magn. 125+).

power because of defect of the mean particle velocity $\delta v$. From the Eq. (5.1) spall zone width $h$ can be expressed in the form:

$$h = \frac{\mu}{\rho C}\left(1+\frac{\delta v}{v}\right)^{-1}. \qquad (5.2)$$

Typical time for spall fracture may be defined as follows:

$$\tau_f = \frac{h}{v} = \frac{\mu}{\rho C v}\left(1+\frac{\delta v}{v}\right)^{-1}. \qquad (5.3)$$

This expression can be rewritten in the form:

$$\frac{\rho C v}{\mu}\left(1+\frac{\delta v}{v}\right)\tau_f = 1,$$

dynamic generalization of which is

$$\frac{\rho C}{\mu}\int_0^{\tau_f}\left(1+\frac{\delta v}{v}\right)v dt = 1 \qquad (5.4)$$

or

$$\frac{1}{\mu}\int_0^{\tau_f}\left(1+\frac{\delta v}{v}\right)\sigma dt = 1, \qquad (5.5)$$

where $\sigma=\rho C v$ is the normal stress at the shock wave front. Equation (5.5) may be considered as a criterion for spallation taking into account an energy exchange between mesolevel-1 and macrolevel.

It can be seen that with the increase of the mean velocity decay $\delta v$ the value of the external stress

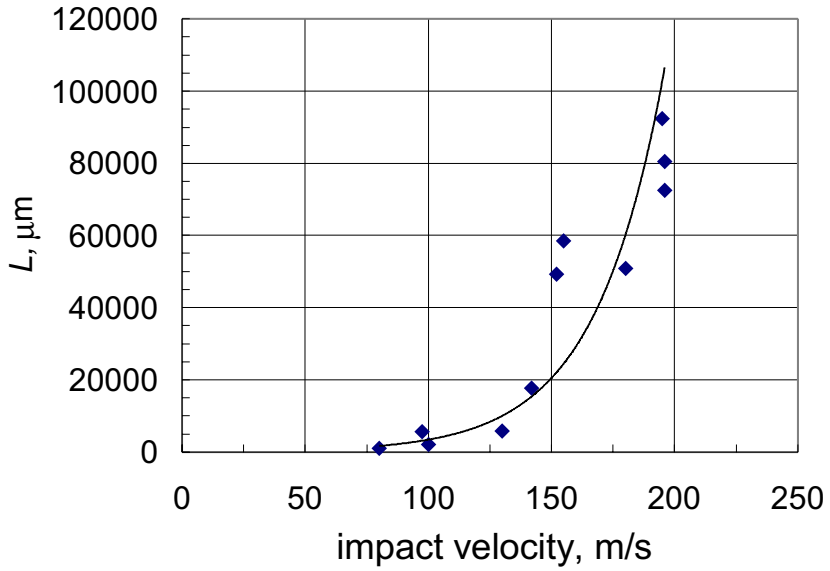


**Fig.4.13.** Dependence of horizon crack length (*H*) on the impact velocity (28Х3СНМВФА steel).

necessary for satisfying the spallation criterion (5.5) decreases. This explains the decrease of pull-back velocity which is seen in all the experiments where $\delta v > \langle \Delta v_1 \rangle$. Equation (5.4) through the equation:

$$\delta v = \frac{1}{2}\frac{d}{dv}D^2 \qquad (5.6)$$

provides a direct coupling between spall strength and the mesoparticle velocity dispersion $D^2$ at the mesolevel-1.

It may be two different situation depending on steadiness of shock wave:

1). In the unsteady shock fronts mesoparticle velocity dispersion increases along the shock front from bottom up to plateau of compressive pulse. One of typical situations of decrease of the free surface velocity at the plateau of compressive pulse is presented in Fig. 1.4a. In this figure we present time-resolved free surface velocity profile for the 30XH4M steel target loaded at the impact velocity of 369 m/s. In case of symmetrical collision (couple: steel impactor – steel target), according to the so-called free surface approximation, there is a following relationship between velocity of impactor $U_{imp}$, mean particle velocity $u$ and free surface velocity of target $U_{fs}$: $U_{imp} = 2v = U_{fs}$. Instead, at the presented in Fig. 1.4a free surface velocity profile pick velocity equals 300 m/s, so the decrease of the free surface velocity at the plateau of compressive pulse equals 69 m/s. Value of this decrease is determined by the rate of change of the particle velocity dispersion according to Eq. (5.6). In this concrete experiment the longitudinal component of diffusion velocity increases over the plastic front from zero to 22 m/s. Diffusion velocity is known to be a three-dimensional value so we may suppose that two other components of the diffusion velocity have the same value. Thus, in the process of pumping over the kinetic energy from macrolevel to mesolevel a longitudinal component of mean particle velocity redistributed between three components of the diffusion velocity. This example shows that when particle velocity dispersion increases along the plastic front up to plateau of compressive pulse the decrease of average particle velocity at the plateau occurs. In accordance with Eq. (5.5) this leads to decrease of the spall-strength of material. Thus, spall-strength of material in unsteady shock loading proves to be smaller than that in the steady waves.

2). In the steady shock waves dispersion achieves its maximum value in the middle of the shock front (see Fig. 1.4 b). During the first half of load front change of the particle velocity dispersion at the mesolevel-1 results in decrease of mean particle velocity at the mesolevel-2. At the middle of load front acceleration of velocity dispersion changes its sign so during the second half of load front there is a decrease of velocity decay

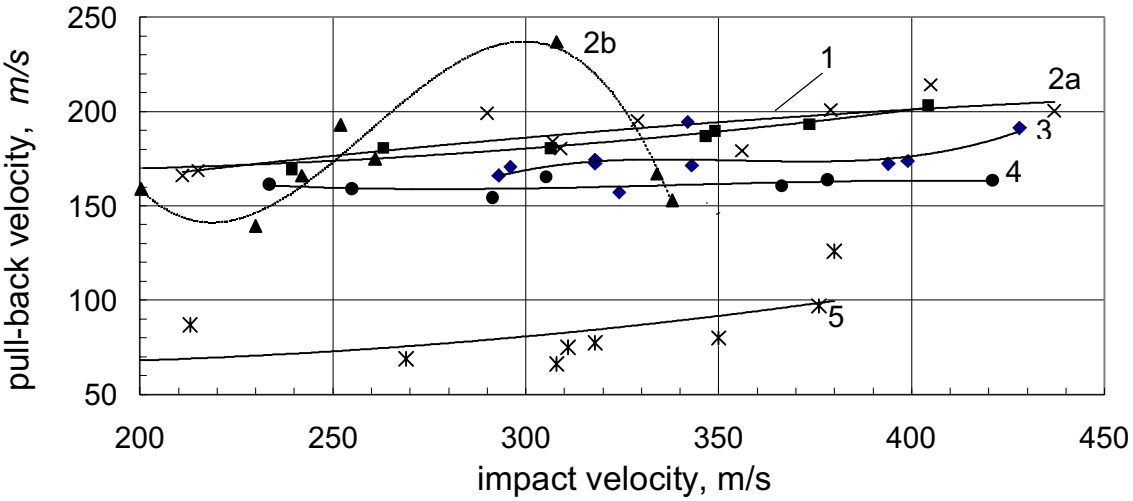


**Fig.5.1.** Free surface velocity profiles in 28X3CHMBΦA steel for two values of the defect free surface velocity: a) $\delta v$ = 80 m/s, b) $\delta v$ = 0.

at the mesolevel-2. Formula (5.6) gives zero value of the velocity decay at the plateau of compressive pulse ($\delta v = 0$). In this case Eq. (5.5) provides a maximum possible spall-strength of material.

Comparing two sets of 38XH3MΦA steel we can conclude that thermal treatment of the second set of steel provides an optimization of dynamic strength properties within the narrow range of the impact velocities from 250 m/s through 330 m/s. Pull-back velocity increases from 185 m/s to 237 m/s, maximum pull-back velocity corresponds to strain rate where $\delta v = \langle \Delta v_1 \rangle$. As for the first set of targets, this equality is satisfied within overall range of impact velocities. In this case the strain-rate behavior of pull-back velocity repeats the behavior of the particle velocity dispersion – it gradually increases with the increase of the impact velocity although the maximum value pull-back velocity remains to be lower than that for the 2-nd set of targets.

In Fig. 5.1 we present dependencies of pull-back velocity for tested steels altogether. One can see that all the kinds of steel, besides the second set of 38XH3MΦA steel, show monotonous increase of pull-back velocity on the impact velocity. We also see that for two kinds of steel – the first sets of 38XH3MΦA steel and 40XCHMA steel – these dependencies lie closely. These steels have different values of Hugoniot elastic limit – 60 m/s for 38XH3MΦA steel and 120 m/s for 40XCHMA steel, respectively. They also have different values of macrohardness: HRc 39 for 38XH3MΦA steel and HRc 55 for 40XCHMA steel. Lastly, microstructure investigations show that mechanisms of dynamic fracture for these steels also are different: ductile fracture for the 38XH3MΦA steel and brittle fracture for the 40XCHMA steel. The only what coincides for these steels is the behavior of the particle velocity dispersion. Values of the diffusion velocity $\langle \Delta v_1 \rangle$ for both steels lie closely velocity decay $\delta v$. Physically this means that there exist optimum conditions for exchange of kinetic energy between mesolevel-1 and mesolevel-2. Processes of relaxation for local stresses flow more quickly than accumulation of local stresses at the mesolevel-2 responsible for dynamic fragmentation of material during spallation. Thus, independently on the kind of resulting mechanism of dynamic fracture the main requirement to material is to initiate a sufficiently effective mechanism for energy exchange between scale levels and provide relaxation of local stresses. In Section 3 we have done an estimation of critical strain rate for nucleation of shear crack during spallation. Its value is determined by the particle velocity dispersion at the mesolevel-2. If the particle velocity dispersion smaller some critical value, the shear cracks have time to heal. Both steels show a small value of the particle velocity dispersion at the mesolevel-2, its value is practically coincides with that at the mesolevel-1. In this case local stresses at the mesolevel-2 haven't time to accumulate. Particle velocity dispersion at the mesolevel-1 characterizes

the local difference in the velocities between adjacent mesovolumes of material. It is else not a shearing or rapture which may be the final stages of this process if its duration is sufficient. Difference in velocities of adjacent mesovolumes else doesn't create the crack. But this difference results in decrease of local stresses because just the local stress through the dynamic impedance $\rho C$ related to the diffusion velocity ($\sigma = \rho C \langle \Delta v_1 \rangle$). Thus, macroscopic strength is determined by the kinetics of microstructure at the mesoscopic scale level. In our concrete case the final reactions of steels are different – brittle for 40XCHMA steel and ductile for 38XH3MΦA steel. Nevertheless, kinetic characteristics for both steels are identical within the impact velocity range of interest. As a result, spall-strength for both materials is practically identical.

Consider now a strength behavior of all the steels altogether. The behavior of kinetic characteristics for the steels is identical. Diffusion velocity $\langle \Delta v_1 \rangle$ and velocity decay $\delta v$ lie practically parallel each other so the rate of change of these characteristics is identical. Therefore local stresses have time to relax during the load front of compressive pulse. In this case difference in spall-strength is determined only by the difference in potential energy of atomic interaction for these material. In case of dynamic straining the potential energy can be related to both the value of elastic precursor and quasistatic strength of material. In Table 12 for comparison we present several strength-characteristics for tested steels. Values of elastic precursor and pull-back velocity are taken for the impact velocity where dependencies $\langle \Delta v_1 \rangle = f(U_{imp})$ and $\delta v = f(U_{imp})$ intersect and $\langle \Delta v_1 \rangle = \delta v$. It has been shown that the 40XCHMA steel is not in optimum state because the intersection of these dependencies doesn't happen within the impact velocity range under investigation. Their intersection may occur at the impact velocity of 695 m/s where the pull-back velocity would achieve the value of 248 m/s. Column 5 gives a ratio of maximum pull-back velocity and that for the rest of the steels. Columns 6 and 7 provide the identical ratio for the $\sigma_b$ and HEL, respectively.

One can see that relative values for pull-back velocity and macrohardness coincide for all the steels besides 38XH3MΦA steel. This means that for all the steel, besides 38XH3MΦA steel, potential energy plays a dominant role in dynamic fracture, while for the latter kinetic energy is also important for dynamic fracture. As for the relative values for Hugoniot elastic limit, a correlation for different steels appears to be not so evident may be because of strain dependence of material.

## 6. CONCLUSIONS

As a result of tests of different kinds of steel and above analysis a total picture of dynamic fracture of heterogeneous materials may presented as follows:

Together with well known quasistatic characteristics of material, such as the quasistatic strength $\sigma_b$ macrohardness HRc, toughness $K_{1c}$ a very important role in dynamic fracture of material belongs to kinetic characteristics of microstructure at the intermediate scale levels.

The first intermediate scale level is the mesolevel-1 (0.1-10 μm). Mobility of elementary carriers of deformation at the mesolevel-1 is responsible for the relaxation of local stresses in dynamically deformed material. The second intermediate scale level is the mesolevel-2 (50-500 μm) This level is responsible for the dynamic fragmentation and fracture of material.

The first kinetic characteristic is the particle velocity dispersion $D^2 = (\Delta v_1^2)$ at the mesolevel-1 or diffusion velocity $\langle \Delta v_1 \rangle$, which are the quantitative measure for the stress relaxation during dynamic deformation and fracture of material. For all the tested steels the character of dependence of spall-strength on the impact velocity appears to be identical with the dependence for the velocity dispersion.

**Table 12.** Comparison of quasistatic and dynamic strength characteristics of steels.

| Steel | $\sigma_b$, MPa | HEL, m/s | Pull-back vel., m/s | $\frac{W_{max}}{W}$ | $\frac{\sigma_b^{max}}{\sigma_b}$ | $\frac{HEL_{max}}{HEL}$ |
|---|---|---|---|---|---|---|
| 40XCHMA | 1870 | 123.5 | 250 | 1 | 1 | 1 |
| 38XH3MΦA | 1220 | 61.1 | 187.5 | 1,33 | 1.53 | 2.02 |
| 4340 | 1260 | 103.3 | 173 | 1.45 | 1.48 | 1.2 |
| 16X11H2B2MΦ | 1150 | 48 | 160 | 1.56 | 1.63 | 2,5 |
| 28X3CHMBΦA | 740 | 48 | 90 | 2.77 | 2.75 | 2.5 |

The second kinetic characteristic is the velocity decay ($\delta v$). Its value characterizes a quantity of the kinetic energy transferred from meslevel-2 to mesolevel-1 and/or back. When a diffusion velocity $\langle \Delta v_1 \rangle$ equals defect of the free surface $\delta v$ this energy exchange is realized in the most effective manner.

The third kinetic characteristic of dynamically deformed material is the diffusion velocity at the mesolevel-2 $\langle \Delta v_2 \rangle$. In this work it is defined as a deviation of the free surface velocity decay $\delta v$ from its average value $\langle \delta v \rangle$.

Stress relaxation takes place at the strain rate where $\langle \Delta v_1 \rangle > \langle \Delta v_2 \rangle$ while an accumulation of local stresses at the mesolevel-2 occurs at the strain rate where $\langle \Delta v_1 \rangle < \langle \Delta v_2 \rangle$. The desirable behavior of kinetic characteristics and $\delta v$ is their equality within overall range of strain rates. In this case spall-strength of material remains invariable. Such a kind of behavior show the 38ХН3МФА steel (set-1), 4340 steel and 16Х11Н2В2МФ steel which structures appear to be in the optimum state. As for the 40XCHMA steel, optimum state of its structure is expected to occur at the impact velocity of 695 m/s where spall-strength of steel may increase by 25%. Thus, measuring the kinetic characteristics in real time permits to predict a way of optimization for heterogeneous material from the point of view of its dynamic strength.

In dynamic processes related to structural phase transitions the most important characteristic becomes not only the mesoparticle velocity dispersion but the rate of its change. Structure phase transition happens when rate of change of diffusion velocity equals the rate of change of the mean particle velocity.

Spall-strength of material decreases with the increase of the velocity decay caused by pumping over the energy from macrolevel to mesolevel.

## ACKNOWLEDGMENTS

We acknowledge the support provided by the V-W Research Project No 1 / 74645 and Special Materials Lmt.

## REFERENCES

[1] J.N. Johnson, O.E. Jones and T.E. Michaels // *Journal of Aplied Physics* **41** (1970) 2770.

[2] V.E. Panin, V.Yu. Grinjaev, T.F. Elsukova and A.G. Ivanchin // *Isvestja Vuzov, Fizika* **6** (1982) 5, In Russian.

[3] V.I. Vladimirov, V.N. Nikolaev and N.M. Priemskii, In: *Physics of strenght and plasticity*, ed. By S..I. Zhurkov (Nauka, Leningrad, 1986) p. 69.

[4] Yu.I. Mescheryakov, In: *Shock Compression of Condensed Matter-1999*, ed. by M.D. Furnish, L.C. Chhabildas and R.S. Nixon (Snowbird, Uh, 1999) p.1065.

[5] S. Cohran and D. Banner // *Journal of Aplied Physics* **48** (1977) 2729.

[6] Yu.I. Mescheryakov, N.A. Makhutov and S.A. Atroshenko // *Journal of the Mechanics and Physics of Solids* **42** (1994) 1435.

[7] L.M. Barker, In: *Shock Compression of Condensed Matter-1999*, ed. by M.D. Furnish, L.C. Chhabildas and R.S. Nixon (Snowbird, Uh, 1999) p. 999.

[8] T.A. Khantuleva and Yu.I. Mescheryakov // *Intern. Journal of Physical Mesomechanics* **2** (1999) 5.

[9] Yu. I. Mescheryakov and A.K. Divakov // *Dymat Journal.* **1** (1994) 271.

[10] J.R. Asay and L.M. Barker // *Journal of Applied Physics* **45** (1974) 2540.

[11] G.E. Duvall // *Irish Journal of Physics and Technics* **7** (1978) 57.

[12] J. Hubburd // *Proceeding of the Royal. Society A* **260** (1961) 114.

[13] W. Horsthemke and R. Lefever, *Noise-induced transitions* (Springer-Verlag, N.Y., 1984).

[14] T.A. Khantuleva, In: *Shock Compression of Condensed Matter-1999*, ed. by M.D. Furnish, L.C. Chhabildas and R.S. Nixon (Snowbird, Uh, 1999) p. 371.

[15] J.J. Gilman // *Applied Mechanics Review* **21** (1968) 767.

[16] D.E. Grady // *Journ. of the Mechanics and Physics of Solids* **36** (1988) 353.